Mon. Not. R. astr. Soc. (1987) **228,** 1–41

Physics of modes in a differentially rotating system – analysis of the shearing sheet

Ramesh Narayan *Steward Observatory, University of Arizona, Tucson, AZ 85721, USA*

Peter Goldreich *California Institute of Technology, Pasadena, CA 91125, USA*

Jeremy Goodman *School of Natural Sciences, Institute for Advanced Study, Princeton, NJ 08540, USA*

Accepted 1987 March 24. Received 1987 February 16

Summary. We analyse the linear non-vortical modes of the shearing sheet, a model compressible two-dimensional fluid system with constant density, constant shear, and Coriolis force. This model has several features found in differentially rotating systems of interest in astrophysics, such as disc galaxies, accretion tori, planetary rings, protostellar nebulae, and possibly even rotating stars.

The linear modal analysis of the shearing sheet leads to an eigenvalue problem based on the Parabolic Cylinder differential equation. A detailed analysis of the solutions is presented. From this we extract the following physical principles: (i) Each mode has an associated 'corotation radius', where the modal pattern is stationary as viewed from a frame moving with the fluid. A mode consists of wave-like disturbances in supersonic 'permitted regions' on either side of corotation, and exponential variation in a sonic 'barrier region' around corotation. (ii) We identify a particular conserved action that is positive for fluid on one side of corotation, and negative on the other side. Because of the change of sign of the action, a wave incident on the corotation barrier is reflected with increased amplitude. The strength of the resulting 'corotation amplifier' depends critically on the amplitude for wave penetration through the barrier. (iii) No instability is possible unless there is feedback introduced into the amplifier. In the shearing sheet, such feedback can take place only at the boundaries. (iv) Unstable modes invariably have equal amounts of positive and negative action, which requires that corotation must occur within the fluid. There are no such restrictions on neutral modes. (v) A semi-infinite shearing sheet has no neutral modes, only unstable modes that are characterized by a resonant 'cavity' between corotation and the edge of the sheet. Growth occurs because the action in the cavity has the opposite sign to that which leaks out to infinity through the corotation barrier. (vi) For a finite shearing sheet with two walls there are two cavities, two amplifiers, and two feedback loops. When tunnelling is small, most of the modes are neutral.

Rare growing modes are produced whenever two stringent phase conditions are simultaneously met, i.e. when both cavities are resonant. (vii) When tunnelling is large, both neutral and unstable modes are common. Most often, one of the cavities takes charge of an unstable mode, and so the modes behave similarly to the semi-infinite system. (viii) When the equilibrium shearing sheet is perturbed slightly by introducing density and/or velocity perturbations, a new qualitative effect occurs in the form of a 'corotation resonance'. Action is absorbed at corotation, and neutral modes are converted into growing or decaying modes. Numerical results are presented to illustrate several of the above features.

1 Introduction

Differentially rotating fluid systems abound in astrophysics: for example stars, accretion discs, protostellar nebulae, planetary rings and spiral galaxies. The evolution of such systems is often controlled by the transport of angular momentum. Accretion discs would not accrete, and protostellar nebulae would not form stars if angular momentum were not exported from inner to outer regions. Yet the nature of the transport mechanism is poorly understood. Microscopic viscosities are usually negligible in astronomical contexts. Magnetic torques are probably often important, but explicit quantitative calculations of their effects are very difficult and have been attempted by only a few investigators, and then only for highly simplified field geometries (e.g. Blandford 1976; Lovelace 1976; Mouschovias 1981; Blandford & Payne 1982; Koen 1986). Therefore, while much has been claimed for magnetic effects, very little has been proven. It seems likely that in some circumstances at least dynamical fluid instabilities play a role. For instance, instabilities are directly visible in spiral galaxies and in planetary rings.

Instabilities involving subsonic shears* are relatively well understood by analogy with laboratory flows. [An extensive review of the theory of incompressible shear flows as of 1979 can be found in Drazin & Reid (1981).] Best understood of all are local and axisymmetric modes, such as Rayleigh's centrifugal instability (both local and axisymmetric), and the Kelvin–Helmholtz instability (non-axisymmetric but quasi-local). Supersonic shear flows present a much more difficult challenge to the experimental physicist and are consequently much less well understood. When such flows are stable against local modes, their remaining instabilities tend to be global and non-axisymmetric. By a combination of numerical experiment and analytical ingenuity, considerable progress has been made in understanding modes in disc galxies [e.g. Julian & Toomre (1966), Lin & Shu (1966), Hohl (1971), Toomre (1977, 1981), to name but a few], planetary rings (e.g. Goldreich & Tremaine 1982), and accretion discs/tori [Papaloizou & Pringle (1984, 1985, 1987, henceforth referred to as PPI, PPII, PPIII)]. The work of Papaloizou & Pringle, in particular, has inspired a number of further investigations, e.g. Blaes (1985), Goldreich, Goodman & Narayan (1986, henceforth, Paper I), Kojima (1986), Blaes & Glatzel (1986), Zurek & Benz (1986), Jaroszinski (1986), Hawley (1987), and Goodman, Narayan & Goldreich (1987, henceforth Paper II). Unfortunately, the details of particular cases are usually sufficiently complex and difficult that they obscure universal aspects common to many systems. The purpose of this paper is to demonstrate these general aspects in a model so simple that it can be thoroughly understood with a minimum of technical effort.

Our model system is the 'shearing sheet' (Goldreich & Lynden-Bell 1965; Goldreich & Tremaine 1978), whose unperturbed state consists of a two-dimensional compressible fluid flowing in straight lines in a Cartesian coordinate frame. The velocity profile is linear with a

*By this we mean instabilities operating over a range Δr in radius such that $\Delta r d \ln \Omega/d \ln r \ll c$, where c might actually be the sound speed but more generally would be the phase velocity of a wave-like disturbance in the system.

constant shear $2A$. The effect of rotation is included through a constant Coriolis parameter Ω. Because of the presence of non-zero A and Ω, the system has most of the essential features of differential rotation. Certain inessential complications that arise due to the variation of A and Ω with radius in real systems are however eliminated. Further, by suitably arranging an external gravitational field, the unperturbed shearing sheet is arranged to have a constant density and sound speed. This filters out effects due to variable density, thus simplifying the problem further.

Despite the simplicity of the shearing sheet, the physics of its modes is rich and fascinating. Section 2 sets up the basic equations to describe linear perturbations of the system. We show that the modal analysis reduces to an eigenvalue problem based on a simple differential equation, the so-called Parabolic Cylinder equation. Section 3 highlights the importance of the 'corotation radius', which is the position at which the modal pattern is stationary as viewed from a frame moving with the fluid. We show that density waves encounter a barrier around the corotation radius, and that this leads to the presence of a wave *amplifier* at corotation (*cf.* also Mark 1976). We argue that all instabilities in the shearing sheet are ultimately fed by the corotation amplifier. We identify a parameter τ that measures the tunnelling amplitude for waves crossing the corotation barrier, and find that the strength of the amplifier depends critically on the value of τ. We also show that a particular 'action' of the wave disturbance is positive on one side of corotation and negative on the other. A more detailed analysis of this important and unifying concept can be found in Appendix A.

In Section 4, we analyse a semi-infinite shearing sheet, with a wall terminating one edge. This system has a one-parameter family of physically meaningful growing modes, and a corresponding family of unphysical decaying modes. There are no neutral modes. In this problem, the boundary condition at the wall effectively provides a feedback which converts the corotation amplifier into an unstable mode. We introduce the important concept of the feedback loop phase. A mode is obtained only when this phase takes on a particular value, modulo 2π. Thus, successive modes are obtained by fitting additional waves within the 'cavity' that exists between corotation and the wall.

Sections 5 and 6 discuss the modes of a finite shearing sheet, confined between two walls. In this problem, whenever the corotation 'radius' lies within the system, there are two amplifiers on the two sides of corotation, each with its own cavity and its own wall to provide feedback. The interaction of these two amplifiers leads to interesting results. In Section 5, which is devoted to the case of small τ, we show that when only one of the cavities satisfies the feedback phase condition, a neutral mode is obtained, whereas in the rare case when both cavities satisfy the phase condition, an unstable mode is obtained. For small τ, most of the modes are neutral, with occasional unstable modes scattered randomly with no obvious pattern of occurrence. Consequently, a probabilistic rather than a deterministic approach is needed in order to catalogue the unstable modes of the system. Section 6 considers the case of large τ, where the amplifiers are very powerful. Here, one amplifier usually overwhelms the effect of the other; consequently, most of the modes behave like the single-amplifier modes of Section 4.

Having analysed the basic shearing sheet in Sections 2–6, we briefly analyse in Section 7 the corotation resonance, an effect that is absent in the shearing sheet, but that is important in some problems. This resonance is present whenever the unperturbed fluid has a non-zero gradient of specific vorticity, and so we analyse the effect of a small perturbation in the density and velocity profile of the shearing sheet. We show that all the neutral modes of the unperturbed shearing sheet become transformed into either weakly growing or weakly decaying modes. The sign of the effect, and its magnitude, can be physically understood in terms of the absorption of positive or negative action at corotation.

In Section 8, we numerically illustrate the theoretical results of the earlier sections by displaying the dispersion curves, and shapes of eigenfunctions, for particular parameters of the shearing

sheet. A noteworthy feature is that, even though we are considering a considerably simpler system here, many of the results are qualitatively very similar to our earlier results on the Papaloizou–Pringle instability in thick accretion tori (Paper I). This illustrates the generality of the effects of differential rotation, and confirms the value of analysing simple models.

A preliminary version of some of our results appeared in an earlier paper (Goldreich & Narayan 1985).

2 The shearing sheet and Parabolic Cylinder equation

We consider a two-dimensional fluid whose velocity $\mathbf{V}$ and surface density Σ obey the following momentum and continuity equations:

$$\frac{d\mathbf{V}}{dt} = -\nabla[\phi(r) - \tfrac{1}{2}\Omega_0^2 r^2] - 2\boldsymbol{\Omega}_0 \times \mathbf{V} - \nabla Q, \tag{2.1}$$

$$\frac{d\Sigma}{dt} + \Sigma \nabla \cdot \mathbf{V} = 0, \tag{2.2}$$

where the operator d/dt is the Lagrangian time derivative, defined by

$$\frac{d}{dt} \equiv \frac{\partial}{\partial t} + (\mathbf{V} \cdot \nabla). \tag{2.3}$$

Equation (2.1), (2.2) describe an ideal barytropic fluid: that is, we have not included any viscosity, and we have taken the two-dimensional pressure P to be a function of Σ, which permits us to define the enthalpy Q through the relation

$$\nabla Q = \frac{\nabla P(\Sigma)}{\Sigma}. \tag{2.4}$$

The fluid is not self-gravitating, but is subject to an external central potential $\phi(r)$. The equations have been written for a frame rotating at angular velocity

$$\boldsymbol{\Omega}_0 \equiv \Omega_0 \hat{\mathbf{k}}, \tag{2.5}$$

where $\hat{\mathbf{k}}$ is a unit vector perpendicular to the $\mathbf{r}$ plane.

If we take the curl of both sides of (2.1) and substitute (2.2), we find

$$\frac{d\zeta}{dt} = 0, \tag{2.6}$$

where ζ, the vorticity per unit surface density, i.e. *specific vorticity*, is defined by

$$\zeta \equiv \frac{(\nabla \times \mathbf{V}) \cdot \hat{\mathbf{k}} + 2\Omega_0}{\Sigma}. \tag{2.7}$$

Thus, every fluid element conserves its specific vorticity.

The equations of the shearing sheet are obtained by making a local approximation to (2.1)–(2.7) and then linearizing. They describe small disturbances of the fluid in the neighbourhood of a point $(r_0, \Omega_0 t)$. The spirit of the local approximation is to treat as constants those quantities that vary only on scales of order r_0. Therefore, instead of the usual polar coordinates r, θ, of inertial space, we now use

$$x \equiv r - r_0,$$

$$y \equiv r_0(\theta - \Omega_0 t), \tag{2.8}$$

and we neglect all terms arising from the curvilinearity of x and y.

It is convenient to choose the angular velocity Ω_0 of the rotating frame to be the equilibrium angular velocity of the fluid at radius r_0. Let us parameterize the local angular velocity profile of the unperturbed fluid as

$$\Omega(r)=\Omega_0\left(\frac{r_0}{r}\right)^q. \tag{2.9}$$

This corresponds to a velocity field in the shearing sheet of the form

$$\mathbf{V}_0=2Ax, \tag{2.10}$$

where the frequency A is assumed to be independent of x and given by

$$2A=-q\Omega. \tag{2.11}$$

(Henceforth, we drop the subscript on Ω_0.) It is useful to remember that $q=2$ corresponds to a constant-angular-momentum disc, $q=3/2$ to a thin Kepler disc, and $q=1$ to a system with a flat rotation curve (constant circular velocity). It is convenient to define the vorticity frequency

$$B\equiv\frac{1}{2r}\frac{d}{dr}(r^2\Omega)\big|_{r_0}=A+\Omega=(2-q)\Omega, \tag{2.12}$$

and the epicyclic frequency

$$\varkappa=\sqrt{4B\Omega}=2(2-q)\Omega. \tag{2.13}$$

Note that A and B are the usual Oort constants, but defined with unusual signs. We regard Ω, A and B as constants of comparable magnitude, except that we occasionally consider the case $B=0$. We assume $\Omega>0$; then, for the usual case of $\Omega(r)$ decreasing outwards and the specific angular momentum $r^2\Omega(r)$ increasing outwards, we have $A<0$, $B>0$.

In the equilibrium shearing sheet, the variation of Σ with x is neglected. This requires that the enthalpy gradient ∇Q should be small compared to Ω^2x. Balancing the other two forces in the right-hand side of equation (2.1), we find that we need a central potential $\phi(r)$ that satisfies

$$\left.\frac{d^2\phi}{dr^2}\right|_{r_0}=\Omega^2+4A\Omega=(1-2q)\Omega^2. \tag{2.14}$$

The density Σ is then constant, and so is the specific vorticity

$$\zeta_0=\frac{2B}{\Sigma}. \tag{2.15}$$

The local constancy of Σ is usually a valid approximation in thin Kepler discs such as planetary rings, and in the discs of spiral galaxies, since the density in these systems generally varies only on the scale of the radius. The approximation is not valid in thick accretion discs/tori, even in the limit of the slender torus (e.g. Paper I), and therefore the shearing sheet model misses certain effects in these systems that have to do with the density gradient. One effect, the corotation resonance, is discussed briefly in Section 7. However, we show in Section 8 that, despite the grossly different density profile, the shearing sheet still manages to reproduce many of the qualitative features of modes in thick tori.

Let us now consider linear perturbations of the constant-density shearing sheet. The first-order Eulerian variations in pressure and surface density are related by the sound speed, c,

$$P'=c^2\Sigma'. \tag{2.16}$$

We write the components of the velocity perturbation as

$$\mathbf{V}'=u\hat{\mathbf{i}}+v\hat{\mathbf{j}}. \tag{2.17}$$

(Notice that we omit the primes on u and v.) Since the equilibrium is independent of t and y, we assume the dependence

$$\Sigma'(x, y, t)=\Sigma'(x)\exp(iky-i\omega t),$$

$$u(x, y, t)=u(x)\exp(iky-i\omega t),$$

$$v(x, y, t)=v(x)\exp(iky-i\omega t), \tag{2.18}$$

where k is real but ω may be complex. The use of the same symbol for the coefficient of the complex exponential and for the full fluid variable should not cause confusion, as the context will always make it clear which is intended.

Let us define

$$\sigma(x)=\omega-2Akx=-2Ak(x-x_c)=q\Omega k(x-x_c). \tag{2.19}$$

The quantity $\sigma(x)$ is the pattern frequency ω, Doppler-shifted to the frame in which the fluid at x is at rest. The pattern is stationary when $\mathrm{Re}(\sigma)=0$, i.e. when viewed from the fluid at the corotation 'radius', $\mathrm{Re}(x_c)$. Note that $\mathrm{Im}(x_c)=-\mathrm{Im}(\omega)/q\Omega k$. Hence, the mode decays when $\mathrm{Im}(x_c)>0$ and grows when $\mathrm{Im}(x_c)<0$.

The linearized forms of (2.1), (2.2), and (2.6) are

$$-i\sigma u-2\Omega v+\frac{c^2}{\Sigma}\frac{d\Sigma'}{dx}=0, \tag{2.20}$$

$$-i\sigma v+2Bu+\frac{ic^2k}{\Sigma}\Sigma'=0, \tag{2.21}$$

$$-i\sigma\frac{\Sigma'}{\Sigma}+\frac{du}{dx}+ikv=0, \tag{2.22}$$

$$-i\sigma\left(\frac{dv}{dx}-iku-\frac{2B}{\Sigma}\Sigma'\right)=0. \tag{2.23}$$

(This makes four equations in three variables, but the equations are not independent: the last follows from the first three.)

In the steps described below we shall divide equation (2.23) through by $-i\sigma$. This implies an integration with respect to time, and restricts us to *non-vertical* perturbations. The 'modes' discarded by this procedure have discontinuous v at corotation. They are vortical (the perturbed vorticity is in the form of a delta function at corotation) and therefore are necessarily neutral, since the specific vorticity has to be conserved. Further, these modes form a continuous spectrum; the discontinuity provides an extra freedom, allowing eigenfunctions to be found with given boundary conditions for any x_c within the flow. Individually, the vortical modes are pathological, as the smallest viscosity would destroy them, but smooth superpositions of them are needed to describe the time evolution from vortical initial conditions. A thorough discussion of discontinuous vortical modes in inviscid plane Couette flow has been given by Case (1960), who shows that these are the only modes allowed in that problem. We shall have nothing more to say about vortical modes in this paper.

Equations (2.21) and (2.23) can be solved for u and Σ:

$$u=-\frac{i}{(c^2k^2+4B^2)}\left(c^2k\frac{dv}{dx}-2B\sigma v\right), \tag{2.24}$$

$$\Sigma'=\frac{\Sigma}{(c^2k^2+4B^2)}\left(2B\frac{dv}{dx}+k\sigma v\right). \tag{2.25}$$

Substituting back in (2.20), we obtain the following differential equation for v

$$\frac{d^2v}{dx^2}+\left[\frac{(\sigma-\varkappa^2)}{c^2}-k^2\right]v=0. \tag{2.26}$$

Let us change the independent variable to

$$X=\left(\frac{4|Ak|}{c}\right)^{1/2}[x-\mathrm{Re}\,(x_c)], \tag{2.27}$$

and define

$$\Lambda=\left(\frac{4|Ak|}{c}\right)^{1/2}\mathrm{Im}\,(x_c), \tag{2.28}$$

$$C=\frac{c^2k^2+\varkappa^2}{4c|Ak|}. \tag{2.29}$$

Equation (2.26) then simplifies to the Parabolic Cylinder differential equation (e.g. Abramowitz & Stegun 1972):

$$\frac{d^2v}{dx^2}+[\tfrac{1}{4}(X-i\Lambda)^2-C]\,v=0. \tag{2.30}$$

Corotation is now at $X=0$, and $-\Lambda$ measures the growth rate of the mode.

Since we are interested in global modes of the shearing sheet, it is necessary to specify boundary conditions for the solution. The most natural boundary condition is to terminate the fluid with a wall parallel to the y-axis at a specified X. We then require the normal velocity u to vanish, which leads via equation (2.24) to

$$\frac{dv}{dX}=\frac{(2-q)}{2}\,\frac{\Omega}{C|k|}(X-i\Lambda)\,v. \tag{2.31}$$

When the system extends to infinity along $+X$ or $-X$, we use the appropriate radiating boundary condition, which requires the solution to behave asymptotically as an outgoing wave.

3 The corotation amplifier

For $\Lambda=0$, the coefficient of v in (2.30) is positive for $|X|>2C^{1/2}$ and negative for $|X|<2C^{1/2}$. The solutions of the differential equation are therefore oscillating or wave-like in the former region and exponential in the latter. We interpret this to mean that there is a 'forbidden region' of width $\pm 2C^{1/2}$ around corotation, with 'permitted regions' on both sides. Waves in the permitted regions can tunnel through the forbidden region, as in all wave problems, and the corresponding transmission coefficient is an important parameter of the problem.

On each side of corotation there are two independent waves possible, an ingoing wave and outgoing wave. Following the notation of Abramowitz & Stegun (1972), we write the asymptotic

forms of these solutions for large $|X|(\gg 2C^{1/2}, \gg |\Lambda|)$ as follows:

$X>0$:

Outgoing:

$$E(X)\simeq \sqrt{\frac{2}{|X|}}\exp\left[\frac{i}{4}(X-i\Lambda)^2\right]\simeq \sqrt{\frac{2}{|X|}}\exp\left(\frac{i}{4}X^2+\frac{1}{2}\Lambda X\right) \tag{3.1}$$

Ingoing:

$$E^*(X)\simeq \sqrt{\frac{2}{|X|}}\exp\left[-\frac{i}{4}(X-i\Lambda)^2\right]\simeq \sqrt{\frac{2}{|X|}}\exp\left(-\frac{i}{4}X^2-\frac{1}{2}\Lambda X\right) \tag{3.2}$$

$X<0$:

Ingoing:

$$E(-X)\simeq \sqrt{\frac{2}{|X|}}\exp\left[\frac{i}{4}(X-i\Lambda)^2\right]\simeq \sqrt{\frac{2}{|X|}}\exp\left(\frac{i}{4}X^2-\frac{1}{2}\Lambda|X|\right) \tag{3.3}$$

Outgoing:

$$E^*(-X)\simeq \sqrt{\frac{2}{|X|}}\exp\left[-\frac{i}{4}(X-i\Lambda)^2\right]\simeq \sqrt{\frac{2}{|X|}}\exp\left(-\frac{i}{4}X^2+\frac{1}{2}\Lambda|X|\right). \tag{3.4}$$

The factor $\sqrt{2/|X|}$ conserves wave action when $\Lambda=0$. Note that the E and E^* waves are not complex conjugates of one another, except when $\Lambda=0$. [We have retained the names E and E^* however in order to be consistent with the notation used by Abramowitz & Stegun (1972).] In writing equations (3.1)–(3.4), certain constant and slowly varying contributions to the phase angles in the exponentials have been neglected. These terms do not affect any of the arguments presented in Sections 3–7. However, in the interests of accuracy, one of the factors, a phase contribution of $\pm\pi/4$, has been included in computing the dashed curves in Figs 4 and 5.

The terms 'ingoing' and 'outgoing' in equations (3.1)–(3.4) are defined with respect to corotation, and the directions refer to the group velocity, i.e. the direction in which wave action is transported. The identification of ingoing and outgoing waves in (3.1)–(3.4) is made by noting that a decaying mode has $\Lambda>0$. For such a mode, the wave action should increase in the direction of propagation because, as one goes farther out, one sees the wave at an earlier time, when it was stronger. Thus, outgoing waves should vary as $\exp(+\frac{1}{2}\Lambda|X|)$, and ingoing waves as $\exp(-\frac{1}{2}\Lambda|X|)$.

If we represent the wave part of the four waves we have discussed as $\exp(i\int k(X)\,dX)$, then the wave-vectors $k(X)$ of the E and E^* waves are given by

$$k_E(X)=\tfrac{1}{2}X, \tag{3.5}$$

$$k_{E^*}(X)=-\tfrac{1}{2}X. \tag{3.6}$$

Consider now the region $X>0$. We have identified the E-wave as outgoing, and as we would expect, this wave has a positive wave-vector k_E, i.e. a wave-vector that is directed outward. So too, the ingoing E^*-wave has an inward-directed wave-vector k_{E^*}. However, these statements are not true for $X<0$. Here, the ingoing E-wave has a negative k_E, i.e. an outward-directed wave-vector, and the E^*-wave has an inward-directed wave-vector. Another way of seeing the inverted behaviour for $X<0$ is to note that $\mathrm{Re}\,[\sigma(x)]$ in equation (2.19) is the pattern frequency seen by the

fluid at x. The component of the group velocity parallel to the y-axis can then be written as

$$(v_{\text{group}})_y = d[\text{Re}(\sigma)]/dk = q\Omega[x - \text{Re}(x_c)]. \tag{3.7}$$

Thus, for $x > \text{Re}(x_c)$, the group velocity is positive, i.e. in the same direction as the wave-vector. However, for $x < \text{Re}(x_c)$, the group velocity is in the opposite direction to the wave-vector.

The physics of the inversion across corotation is dealt with in some detail in Appendix A. There we use Noether's theorem to derive the second-order perturbed angular momentum of the shearing sheet. By adding the divergence of a flux that vanishes on the boundaries of the shearing sheet, we then obtain the following particular action density (see equation A.25)

$$\varrho_* = \frac{k\Sigma[\text{Re}(\sigma)]}{2}\left(|\xi^x|^2 + |\xi^y|^2 + \frac{c^2\Omega}{|\sigma|^2 B}\left|\frac{\partial \xi^x}{\partial x} + \frac{\partial \xi^y}{\partial y}\right|^2\right), \tag{3.8}$$

where ξ^x and ξ^y are Lagrangian displacements which can be written in terms of the Eulerian velocity components u and v by means of equations (A.14). The action density ϱ_* has the following properties:

(i) When averaged over y it satisfies a conservation law (equation A.3)

$$2[\text{Im}(\omega)]\varrho_* + \frac{\partial j_*}{\partial x} = 0, \tag{3.9}$$

where the flux j_* is given by (equation A.26)

$$j_* = -\frac{c^2 k\Sigma}{2}\text{Re}\left[i\left(1 + \frac{\Omega\sigma^*}{B\sigma}\right)\left(\frac{\partial \xi^x}{\partial x} + \frac{\partial \xi^y}{\partial y}\right)\xi^{x*}\right]. \tag{3.10}$$

(ii) The flux j_* vanishes on the boundaries of the system if either $\xi^x = 0$ (rigid wall boundary condition) or $\nabla \cdot \xi = 0$ (constant pressure boundary condition). Therefore, by equation (3.9), there is a global conservation law on the total action, whenever the system satisfies one of these two physical boundary conditions.

(iii) For the usual choice of signs, $k > 0$, $A < 0$, $B > 0$, the action density ϱ_* is positive for $X > 0$ and negative for $X < 0$. This makes the corotation radius a very important location in the system.

We will frequently use the above properties of the action density ϱ_* in the rest of the paper. Here we note that the physical reason for the action being negative in the region $X < 0$ is that the wave pattern moves *backward* with respect to the fluid in this region of the system. Pierce (1974) gives an excellent discussion of backward-moving waves and explains how they can have negative momentum or angular momentum. Indeed, the negative sign of action for $X < 0$ is the underlying reason for the group velocity being directed in the opposite direction compared to the wave-vector in this region of the fluid.

The identification of positive and negative action regions depends critically on the sign of $2Ak = -q\Omega k$. The above discussion is for the standard case, $A < 0$, $k > 0$, i.e. a shear with velocity decreasing for large X, and a wave propagating in the $+y$ direction. A general statement, which is not restricted to the above choice of signs, is as follows: The wave has positive action in those regions where the fluid velocity is less than that of the pattern, when measured with respect to the direction of propagation of the pattern, and negative action in regions where the fluid goes faster. Thus, in differentially rotating discs of interest in astronomy, waves have negative action at radii less than the corotation radius, where $\Omega(r)$ is larger, and positive action outside corotation.

Abramowitz & Stegun (1972) give the following matching conditions for the Parabolic Cylinder equation for the waves discussed above:

$$\sqrt{1 + \exp(2\pi C)}\, E(X) = \exp(\pi C)\, E^*(X) + iE^*(-X). \tag{3.11}$$

Let us define

$$\tau = \exp(-\pi C). \tag{3.12}$$

We note that τ measures the amplitude for wave tunnelling through the corotation barrier. Equation (3.11) can now be rewritten as

$$E^*(X) - \sqrt{1+\tau^2}E(X) = -i\tau E^*(-X). \tag{3.13}$$

This equation has a particularly transparent physical interpretation. It says the ingoing wave $E^*(X)$ of unit amplitude interacts with the forbidden region around corotation to produce a transmitted wave of amplitude τ and a reflected wave of amplitude $\sqrt{1+\tau^2}$. The transmitted amplitude τ is exactly what we expect in a WKB barrier penetration analysis of the forbidden region. The *increased* reflected amplitude is however a counter-intuitive result, and arises because of the opposite sign of action on the two sides of corotation. The incoming wave $E^*(X)$ in (3.10) has unit flux of positive action, while the transmitted wave $E^*(-X)$ has a flux of negative action of magnitude τ^2. Therefore, conservation of total action demands that the reflected wave should have a flux of positive action of magnitude $1+\tau^2$, i.e. an amplitude $\sqrt{1+\tau^2}$. By symmetry, this 'corotation amplifier' works equally well for incident negative action waves.

All unstable modes in the shearing sheet owe their origin ultimately to the corotation amplifier. There are three consequences of this statement:

(i) Unstable modes must have corotation within the system, i.e. there is always some fluid that corotates with the pattern.

(ii) Since the total action must be conserved, and since the amplitude of unstable modes varies with time, therefore these modes must have zero net action. Thus, the positive wave action in the $X>0$ region of the fluid must be exactly cancelled by the negative action in the $X<0$ region. We call these 'balanced' modes.

Neither of the above conditions applies to a neutral mode. Its corotation can occur outside the fluid, and when it occurs within the fluid, the mode can be 'unbalanced', and can have predominantly one sign of action.

(iii) Unstable modes are obtained when the fluid system, in a sense, becomes an oscillator. This means the corotation amplifier needs feedback, i.e. there must be an agency to turn back some of the outgoing action to close the feedback loop. In this paper, we assume that the system has walls to provide the necessary reflection of wave action.

4 Modes with a single wall

We consider first a simple case, where the shearing sheet extends indefinitely toward $+x$, but is terminated by a wall with appropriate boundary conditions at some finite $-x_0$. Different modes of this system will be characterized by different locations of corotation. However, in the modified problem of equation (2.30), corotation is constrained to be at $X=0$, and so we can equivalently consider different locations, $-X_-$, for the wall.

Since the fluid extends to infinity along positive X, the solution for $X>0$ must be in the form of an outgoing wave, namely $E(X)$. We must therefore consider the following modification of equation (3.13)

$$E(-X) - \sqrt{1+\tau^2}E^*(-X) = i\tau E(X). \tag{4.1}$$

The boundary condition at the wall at $-X_-$ is given in equation (2.31), and involves a linear combination of v and dv/dX. However, in the WKB regime in which we are interested, there are many wavelengths between corotation and the boundary, and the precise boundary condition is

not qualitatively important. To keep matters simple, we will assume the following simpler boundary condition,

$$v(-X_-)=0. \tag{4.2}$$

Substituting equations (3.3) and (3.4) into (4.1), and applying the boundary condition (4.2), we find

$$\exp\left(\frac{i}{2}X_-^2\right)\exp(-\Lambda X_-)=-\sqrt{1+\tau^2}. \tag{4.3}$$

This equation requires two conditions to be simultaneously satisfied. Equating the phases of the two sides, we obtain

$$\psi\equiv\tfrac{1}{2}X_-^2 \text{ modulo } 2\pi=0, \tag{4.4}$$

which states that each successive solution for X_- involves an extra phase of 2π for the round trip from corotation to the wall and back. Equating the moduli of the two sides of (4.3), we next obtain

$$\Lambda=-\frac{1}{2X_-}\ln(1+\tau^2). \tag{4.5}$$

The negative sign of Λ implies a growing mode. Thus, all modes of the single-wall shearing sheet are growing modes.

The physics of the growth is simple. We have a *resonant* 'cavity' between corotation at $X=0$ and the wall at $X=-X_-$. This cavity is filled with negative action, while positive action is continuously leaking out of it through the corotation barrier and flowing away toward $X=+\infty$. To conserve total action, the negative action in the cavity has to grow. The wall at $-X_-$ thus provides the feedback that is necessary to convert the corotation amplifier into an unstable oscillator.

The magnitude of the growth rate can also be understood physically. The growth rate is given by $\mathrm{Im}(\omega)$ which for the above Λ is

$$\mathrm{Im}(\omega)=\frac{c}{4x_-}\ln(1+\tau^2), \tag{4.6}$$

where $x_-=(c/4|Ak|)^{1/2}X_-$ is the physical distance between corotation and the wall. Let us define t_s to be the time taken by a sound wave to travel up and down the cavity once,

$$t_s=2x_-/c. \tag{4.7}$$

The factor by which the action in the cavity grows during one sound-crossing time is thus

$$\exp[2\,\mathrm{Im}(\omega)\,t_s]=1+\tau^2, \tag{4.8}$$

which is precisely what we expect for an amplifier that reflects a wave of unit flux of action into a wave of flux $1+\tau^2$.

Finally, we explicitly demonstrate the 'balanced' nature of these modes. At any instant, the total positive action of the outgoing wave outside the cavity is

$$\varrho_+\propto\tau^2\int_0^\infty\exp(\Lambda X)\,dX=2\tau^2X_-/\ln(1+\tau^2). \tag{4.9}$$

The negative action within the cavity at the same instant is

$$\varrho_-\propto\int_{-X_-}^0[\exp(-\Lambda|X|)+(1+\tau^2)\exp(\Lambda|X|)\,dX=2\tau^2X_-/\ln(1+\tau^2). \tag{4.10}$$

The net action is thus seen to be zero. Although the expressions for the waves written in equations (3.1)–(3.4) are really valid only for large $|X|$, they can be consistently used down to $X=0$ in arguments such as the above.

In PPIII a similar, though more complicated, fluid system is considered and a WKB radiation condition is imposed on one side of corotation. These authors have reached conclusions similar to those of the present section – in particular, that all modes are weakly growing. They have also demonstrated that such one-walled modes can be relevant to the stability of accretion tori even if they have finite outer radii. [See also the discussion surrounding equations (5.1.28)–(5.1.30) below and in Section 6.]

The solutions discussed in this section satisfy the physically correct boundary condition of an outgoing wave for $X>0$. Mathematically, however, there are also solutions with an ingoing wave for $X>0$. These correspond to the case when positive wave action is pumped in from large positive X with a precisely tuned decay of wave amplitude so as to produce a 'mode'. These solutions give the decaying counterparts of the physically interesting growing modes discussed above.

5 Modes with two walls – small tunnelling probability case

We are now in a position to analyse a more interesting problem, namely a shearing sheet extending over a finite range of x between two walls. This system is somewhat complicated, and so we divide our discussion into two sections, treating two limits of particular interest. In this section we consider the case $\tau \ll 1$. Since τ measures the probability of barrier penetration, this corresponds to weak interaction between the two sides of corotation, i.e. we have weak amplification. In Section 6, we discuss the limit $\tau \gg 1$, which corresponds to strong interaction, and strong amplification.

Even within the $\tau \ll 1$ case, we consider two sub-cases separately. In Section 5.1, we look at the case when the two walls are sufficiently far apart that the WKB phase from a central corotation to the walls is several cycles. [Alternatively, for fixed walls, this corresponds to assuming a sufficiently large value of k, see equations (3.5), (3.6) and (2.27).] In this WKB limit we can use the E and E^* waves (equations 3.1–3.4) as we did in the single-wall case of Section 4. In Section 5.2, we consider the opposite limit when k is sufficiently small that the mode has no nodes at all.

5.1 LARGE WAVE-VECTOR, OR WKB, CASE

As before, a system with fixed walls and variable corotation 'radius' is mapped onto a problem where corotation is fixed at $X=0$ and the walls are at $+X_+$ and $-X_-$. The total width is $W=X_++X_-$. The system now has two cavities, one on each side of corotation, with full feedback being provided by the two walls.

Since we are free to use any normalization for the mode amplitude, we assume that a mode consists in the $X>0$ cavity of an outgoing wave $\tau E(X)$ and an ingoing wave $\mathscr{A}\tau E^*(X)$. As in Section 4, we will, without loss of generality, modify the boundary condition to $v=0$, since it simplifies the analysis considerably. Note, however, that in the numerical work of Section 8, the correct boundary condition is used, namely $u=0$. Applying the condition $v=0$ at $X=X_+$ and using the expressions for $E(X)$ and $E^*(X)$ given in equations (3.1) and (3.2), we obtain

$$\mathscr{A}=-\exp(i\phi+\Lambda X_+), \tag{5.1.1}$$

where the phase ϕ in the $X>0$ cavity is defined to be

$$\phi=\tfrac{1}{2}X_+^2 \text{ modulo } 2\pi. \tag{5.1.2}$$

(Compare with equation 4.4 which defines the analogous phase ψ of the $X<0$ cavity.) By suitably rewriting equation (3.13), the waves $\tau E(X)$ and $\mathscr{A}\tau E^*(X)$ can be matched to waves in the $X<0$ cavity as follows,

$$\tau E(X)=-iE(-X)+i\sqrt{1+\tau^2}E^*(-X), \tag{5.1.3}$$

$$\mathscr{A}\tau E^*(X)=-i\mathscr{A}\sqrt{1+\tau^2}E(-X)+iE^*(-X). \tag{5.1.4}$$

The solution in the $X<0$ cavity is the sum of the right-hand sides of (5.1.3) and (5.1.4) with $\mathscr{A}$ given in (5.1.1). Applying the boundary condition $v=0$ at $X=-X_-$ to this solution, we obtain

$$1-\sqrt{1+\tau^2}\exp(\Lambda W r_+ + i\phi)-\sqrt{1+\tau^2}\exp(\Lambda W r_- - i\psi)+\exp(\Lambda W + i\phi - i\psi)=0, \tag{5.1.5}$$

where ψ is defined in equation (4.4), and the dimensionless ratios r_+, r_- are given by

$$r_+=X_+/W, \tag{5.1.6}$$

$$r_-=X_-/W. \tag{5.1.7}$$

Equation (5.1.5) is exact in the WKB regime being considered here, and can be applied for all values of τ.

Let us now specialize to $\tau\ll 1$, i.e. weak barrier penetration. We will assume (this is verified *a posteriori* in 5.1.17) that unstable modes have

$$|\Lambda W|\sim\tau. \tag{5.1.8}$$

We can then expand (5.1.5) and retain terms up to order τ^2. Thus,

$$\{\exp(i\phi)+\exp(-i\psi)-\exp[i(\phi-\psi)]-1\}+[\exp(i\phi)+\exp(-i\psi)]\frac{\tau^2}{2}$$
$$+\{r_+\exp(i\phi)+r_-\exp(-i\psi)-\exp[i(\phi-\psi)]\}\Lambda W$$
$$+\{r_+^2\exp(i\phi)+r_-^2\exp(-i\psi)-\exp[i(\phi-\psi)]\}\frac{(\Lambda W)^2}{2}=0. \tag{5.1.9}$$

Consider first neutral modes, which have $\Lambda=0$. We require

$$[\exp(i\phi)-1][1-\exp(-i\psi)]+[\exp i\phi)+\exp(-i\psi)]\frac{\tau^2}{2}=0. \tag{5.1.10}$$

Since τ is small, either ϕ or ψ must be close to 0 in order to satisfy this equation. Assuming ϕ to be small, we have

$$\phi=\frac{\tau^2}{2}\cot\frac{\psi}{2}. \tag{5.1.11}$$

There is an analogous result when ψ is small. For both ϕ and ψ small, we have

$$\phi\psi=\tau^2, \tag{5.1.12}$$

which is a hyperbola. These phase conditions are illustrated in Fig. 1 in the $\phi\psi$-plane. Note that, in contrast to the single-wall problem, here we do have neutral modes. Also, note that the phase conditions for neutral modes are independent of r_+ or r_-.

The phase conditions (5.1.11), (5.1.12) pertain to 'two-cavity' neutral modes, where corotation lies within the fluid. There are, in addition, other 'single-cavity' neutral modes, whose corotations lie outside the walls. For instance, if X_- is negative (which corresponds to corotation occurring to

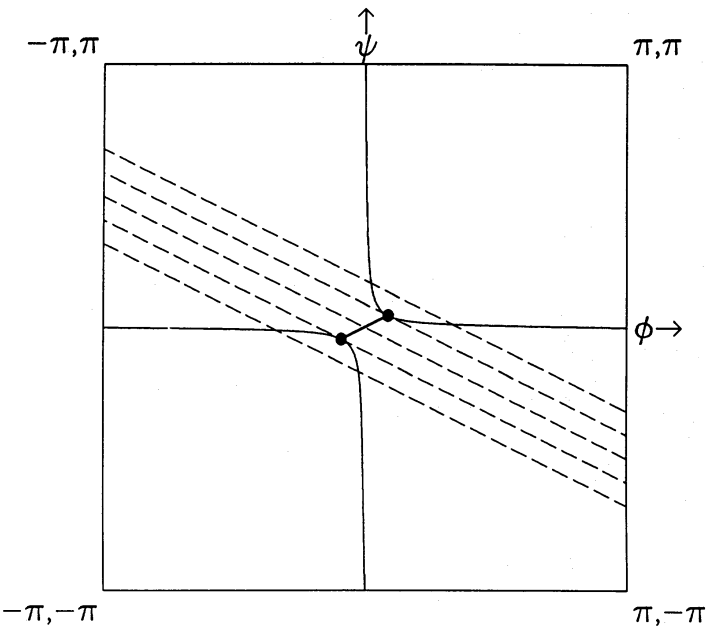

Figure 1. $\phi\psi$-phase diagram for a case with small tunnelling probability. ϕ and ψ vary from $-\pi$ to π and are plotted horizontally and vertically, respectively. The two hyperbola-like curves correspond to the neutral branch for $\tau=0.2$. The straight line connecting the two dots is the unstable branch (see equation 5.1.16) when $r_-=1/3$ and $r_+=2/3$, i.e. $r_-/r_+=1/2$. The dashed lines correspond to $\phi\psi$ pairs obtained by tuning the location of corotation, for this value of r_-/r_+ (see equation l5.1.18). Different dashed lines are obtained as the total width, W, of the system is varied.

the left of the left wall), then we require the phase condition

$$\tfrac{1}{2}(X_+^2-X_-^2)=2n\pi, \qquad n=1, 2, \ldots . \tag{5.1.13}$$

Similarly, if corotation is to the right of the fluid, i.e. $X_+<0$, we require for a neutral mode

$$\tfrac{1}{2}(X_-^2-X_+^2)=2n\pi, \qquad n=1, 2, \ldots . \tag{5.1.14}$$

These modes correspond simply to standing sound waves in a shearing system.

For unstable modes, corotation has to lie within the fluid (see Section 2), and so X_+, X_- are both >0. We assume that ϕ, $\psi\sim\tau$ (verified below in 5.1.17), and write equation (5.1.9) appropriately

$$(\tau^2-\phi\psi)+i(\psi r_+-\phi r_-)\,\Lambda W-r_+r_-(\Lambda W)^2=0. \tag{5.1.15}$$

This is solved by

$$\frac{\psi}{\phi}=\frac{r_-}{r_+}, \tag{5.1.16}$$

$$\Lambda W=\pm\left(\frac{\tau^2-\phi\psi}{r_+r_-}\right)^{1/2}. \tag{5.1.17}$$

We note that unstable modes occur in growing/decaying pairs. In the $\phi\psi$-phase diagram of Fig. 5.1, the unstable branch is situated close to the origin, ϕ—$\psi=0$, and takes the form of a straight line of slope r_-/r_+. The growth/decay-rate goes to zero when $\phi\psi=\tau^2$, which corresponds to the two points where this line meets the neutral branch.

A feature of the unstable branch, not found in the neutral branch, is that it is described on the phase diagram by a curve that depends on the ratio r_-/r_+. There is a reason for this. Consider a

problem where the distance between the two walls W is fixed. Moving the position of corotation corresponds to simultaneously changing X_+ and X_- with $dX_+ = -dX_-$. This then corresponds to a straight line trajectory on the phase diagram described by

$$\left(\frac{d\psi}{d\phi}\right)_W = -\frac{r_-}{r_+}. \tag{5.1.18}$$

Intersections of this line with the neutral or unstable branches correspond to appropriate modes. Now, the unstable and neutral branches meet at a point given by

$$\phi = (r_+/r_-)^{1/2}\tau, \qquad \psi = (r_-/r_+)^{1/2}\tau, \tag{5.1.19}$$

and the slope of the neutral branch at this point is

$$\left(\frac{d\psi}{d\phi}\right)_{\text{neutral}} = -\frac{r_-}{r_+}. \tag{5.1.20}$$

Note the equality of (5.1.18) and (5.1.20). This has the following consequence. Consider the effect of slowly moving the walls apart. The phase pairs accessible by tuning the location of corotation are described by lines of slope (5.1.18) but translated parallel to one another for different choices of W. We have shown this schematically in Fig. 1. The modes of the system are where these lines intersect the neutral and unstable branches. Thus, as W changes, two neutral modes merge to produce a pair of unstable modes, and vice versa. This happens only because the slopes (5.1.18) and (5.1.20) are equal. If the two were not equal, then there would be values of W at which two unstable modes would be created suddenly, without the destruction of two other modes, and there would be no conservation of the number of modes. Thus it is essential for the slope of the unstable branch in the $\phi\psi$-diagram to vary with r_-/r_+.

For r_+, r_- not too different from 1/2, equations (5.1.16) and (5.1.17) imply that $\phi \sim \psi \sim 0(\tau)$. Thus, both cavities need to satisfy the 'quantum' phase condition to rather high precision, i.e. both cavities need to be simultaneously resonant. Since for small τ the probability of this happening in the neighbourhood of any W and (r_-/r_+) is small, we deduce that the majority of phase space is occupied by neutral modes, which require only one of the two cavities to be resonant. Note the contrast with the single-wall problem. In that case, there is only one cavity, but every time the cavity becomes resonant a growing mode is obtained.

The rarity of unstable modes for small τ means that we should employ a *probabilistic* rather than a *deterministic* approach in predicting the occurrence of instabilities. Let us suppose that for some value of k, the two cavities are simultaneously resonant for some position of corotation, leading to a pair of unstable modes. Even for a small change in k, it will be impossible to satisfy the resonance in both cavities, which means the unstable modes will be replaced by two neutral modes. In effect, all memory of the instability is lost, and as k is varied, the next unstable pair could occur with corotation anywhere in the system. It is this loss of memory which leads us to conclude that a statistical approach is appropriate in cataloguing the instabilities of the system.

The maximum growth rate in the two-wall problem occurs when $\phi = \psi = 0$,

$$|\Lambda|_{\max} = \frac{\tau}{W(r_+ r_-)^{1/2}} = \frac{\tau}{(X_+ X_-)^{1/2}}. \tag{5.1.21}$$

We see that Λ is of order τ, in contrast to the single-wall problem where, for small τ, $\Lambda \sim \tau^2$. Thus the reduced probability of obtaining an unstable mode in the two-wall problem is compensated by an increased growth rate, conserving total growth rate.

Consider next the action stored in the two cavities. From equations (5.1.1)–(5.1.4) we see that

the solutions in the two cavities are given by

$$X>0: \tau E(X)-\exp(i\phi+\Lambda X_+)\,\tau E^*(X) \tag{5.1.22}$$

$$X<0: -i[1-\sqrt{1+\tau^2}\exp(i\phi+\Lambda X_+)]\,E(-X) + i[\sqrt{1+\tau^2}-\exp(i\phi+\Lambda X_+)]\,E^*(-X). \tag{5.1.23}$$

Let us consider the neutral branch, with $\Lambda=0$ and $\phi\psi=\tau^2$. By means of an analysis similar to that in equations (4.9) and (4.10) we obtain

$$\varrho_+ \propto X_+, \tag{5.1.24}$$

$$\varrho_- \propto \frac{\phi}{\psi} X_-. \tag{5.1.25}$$

The ratio of the two actions is

$$\frac{\varrho_+}{\varrho_-} = \frac{\psi}{\phi}\frac{X_+}{X_-}. \tag{5.1.26}$$

Let the neutral branch correspond to the $X<0$ cavity being resonant, i.e. having $\psi\sim 0$, ϕ arbitrary. We find that $\varrho_->\varrho_+$, i.e. most of the action is concentrated in this cavity. So too when $\phi\sim 0$, most of the action resides at $X>0$. Thus, we can make the following statements about neutral modes:

(i) They are characterized by a single resonant cavity.
(ii) They have most of their action density in this cavity.
(iii) They are 'unbalanced', with a net positive or negative action depending on which cavity is resonant.

The two cavities in the neutral mode have equal amounts of action when

$$\frac{\psi}{\phi} = \frac{X_-}{X_+} = \frac{r_-}{r_+}. \tag{5.1.27}$$

By (5.1.16), this is the point at which the unstable branch meets the neutral branch, and is exactly what the physics of the problem dictates, since unstable modes have to be 'balanced'. Substituting (5.1.16) and (5.1.17) into (5.1.22) and (5.1.23) and with a little work, it can be shown that, in addition to this point of intersection, the whole of the unstable branch has equal amounts of positive and negative action.

We make one last comment, comparing the single- and two-wall problems. Let us assume $X_+>X_-$ and write (5.1.21) as

$$|\Lambda| = \frac{\tau}{X_-}\left(\frac{r_-}{r_+}\right)^{1/2}. \tag{5.1.28}$$

As the wall at X_+ recedes from corotation, the growth rate decreases until, at

$$\frac{r_-}{r_+} = \frac{\tau^2}{4}, \tag{5.1.29}$$

the growth rate equals that of the single-wall problem (equation 4.5 for small τ). This is also the extreme cavity ratio at which a tangent point can be found on the neutral branch, as shown by

$$\left|\frac{d\psi}{d\phi}\right|_{\mathrm{W,min}} = \left|\frac{r_-}{r_+}\right|_{\mathrm{min}} = \left|\frac{d\psi}{d\phi}\right|_{\mathrm{neutral},\phi=\pi} = \frac{\tau^2}{4}, \tag{5.1.30}$$

where the last relation is obtained by differentiating (5.1.10). All this suggests that for $r_-/r_+<\tau^2/4$ something new has to happen. In fact, in this regime the two-wall system behaves effectively like a single-wall system because, by the time a wave goes from corotation to the wall and back in the long cavity, it has bounced a large number of times in the short cavity and the action in this cavity has grown so much that the feedback in the long cavity becomes irrelevant. The 'phase transition' from two-wall to single-wall behaviour is treated in greater detail in Section 6.

5.2 SMALL WAVE-VECTOR – 'PRINCIPAL' OR NODELESS MODE

In Section 5.1 we considered the WKB regime where, for a given large wave-vector k, the two-wall system has a large number of modes with corotation within the fluid. Most of these modes are neutral and a few are unstable. Here we consider the limit of small k. Using the results of Paper I on slender tori as a guide, we expect only a pair of modes in this case, the so-called 'principal branch', with corotation exactly at the mid-point between the walls.

Let the 'Mach number' of the flow be M, defined to be the velocity difference from the centre to either wall. The separation w between the walls is then given by

$$2Aw=2Mc. \tag{5.2.1}$$

In terms of the dimensionless coordinate X, the walls are at

$$X=\pm MX_0, \tag{5.2.2}$$

where we have defined

$$X_0=(kw/M)^{1/2}. \tag{5.2.3}$$

For sufficiently small k, X_0 is small, and equation (2.30) shows that no nodes are possible in the solution for v.

Two regimes need to be considered, depending on the magnitude of

$$C=\frac{X_0^2}{4}+\frac{2(2-q)}{q^2X_0^2}. \tag{5.2.4}$$

Consider first the case $q=2$, when $C=X_0^2/4$ is a small quantity. This special case corresponds to having zero epicyclic frequency $\varkappa$. Hence, the two Lindblad 'resonances', located at the points where $\sigma(X)=\pm\varkappa$, are degenerate and occur at $X=0$. (The term 'resonance' is actually misleading in this context, since the shearing sheet has no singularity at these points.) We can now develop a power-series solution for v, using some obvious symmetry requirements on the solution

$$v(X)=\left\{1+\frac{(\Lambda^2+X_0^2)}{8}X^2+\frac{1}{12}\left[\frac{(\Lambda^2+X_0^2)^2}{32}-\frac{\Lambda a}{2}-\frac{1}{4}\right]X^4+\ldots\right\}$$
$$+i\left\{ax+\left[\frac{(\Lambda^2+X_0^2)}{24}a+\frac{\Lambda}{12}\right]X^3+\ldots\right\}. \tag{5.2.5}$$

Let us apply at $X=\pm MX_0$ the boundary condition (2.31), which simplifies in this case to $dv/dX=0$. From the imaginary part we obtain

$$a=-\tfrac{1}{4}\Lambda M^2X_0^2. \tag{5.2.6}$$

Substituting this in the real part, we get

$$\Lambda=\pm\left(\frac{M^2}{3}-1\right)^{1/2}X_0. \tag{5.2.7}$$

Thus, there is a pair of unstable modes, one growing and one decaying, whenever

$$M>\sqrt{3}. \tag{5.2.8}$$

This shows that supersonic shear is a requirement for the presence of the instability corresponding to the principal branch. This is true also of the WKB modes of Section 5.1, since they need permitted regions on either side of corotation.

The above analysis requires C to be small. It could be applied even for $q\lesssim 2$, so long as $1\gg X_0^4\geq 8(2-q)/q^2$, which is the condition that the Lindblad resonances should lie well within the system. The boundary condition would be more complicated (see equation 2.31).

Let us consider instead the other regime, $q<2$, $X_0\to 0$. Here $C\sim 2(2-q)/q^2X_0^2$ becomes very large, and a power series solution is not appropriate. Instead, we neglect $(X-i\Lambda)^2/4$ compared to C in (2.30) and write

$$\frac{d^2v}{dX^2}=\frac{C'}{X_0^2}v, \tag{5.2.9}$$

where

$$C'=2(2-q)/q^2. \tag{5.2.10}$$

By the same symmetry arguments as before, the solution must be of the form

$$v(X)=\cosh\left(C'^{1/2}\frac{X}{X_0}\right)+ia\sinh\left(C'^{1/2}\frac{X}{X_0}\right). \tag{5.2.11}$$

Now we apply the boundary condition (2.31) at $X=MX_0$. The imaginary part gives

$$a=\left[M\tanh\left(C'^{1/2}M\right)-\frac{qC'^{1/2}}{(2-q)}\right]^{-1}\frac{\Lambda}{X_0}. \tag{5.2.12}$$

Substituting in the real part, we obtain

$$\Lambda^2=-\frac{2}{2-q}-M^2+\frac{2^{3/2}M}{(2-q)^{1/2}}\coth\left[\frac{2^{3/2}(2-q)^{1/2}M}{q}\right]. \tag{5.2.13}$$

For unstable modes we require $\Lambda^2>0$. It can be verified that there are no solutions for $q<2$ if $M<\sqrt{3}$, the same condition as (5.2.8). For $M>\sqrt{3}$, unstable modes exist for $q<2$ down to some $q_{\min}$ which depends on M. For $M=2$, $q_{\min}=1.403$, and for $M=5$, $q_{\min}=1.889$. These features are explored in greater detail in the numerical work of Section 8.

6 Modes with two walls – large tunnelling probability case

We consider in this section the limit when the tunnelling amplitude $\tau=\exp(-\pi C)$ is large compared to 1. This requires negative C, which by equations (2.29) and (2.13) requires $q>2$. This is not an interesting regime for fluid discs since angular momentum would decrease outwards, leading to a local instability by the Rayleigh criterion. However, a $\tau\gg 1$ shearing sheet is a good model to simulate the effect of a strong amplifier. Instabilities in self-gravitating discs such as spiral galaxies are probably controlled by the 'swing amplifier', which can produce amplifications of up to a factor ~100 (Toomre 1981). The analysis of this section should be viewed as a way to obtain a qualitative understanding of such systems.

The basic equation we need to solve is again (5.1.5). Let us consider neutral modes first. Setting $\Lambda=0$, we obtain

$$\sqrt{1+\tau^2}\,\{\exp[i(\phi+\psi)]+1\}-[\exp(i\phi)+\exp(i\psi)]=0. \tag{6.1}$$

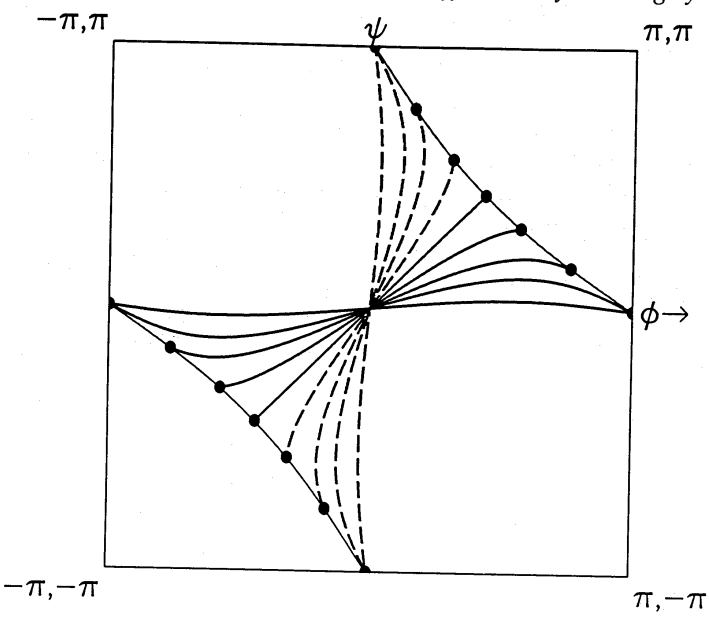

Figure 2. $\phi\psi$-phase diagram for a case with large tunnelling probability. ϕ and ψ vary from $-\pi$ to π and are plotted horizontally and vertically, respectively. The thin solid lines correspond to the neutral branch for $\tau=5$. The various thick lines connecting pairs of dots correspond to unstable branches. The line of slope 1 corresponds to $r_-=r_+=0.5$. Succeeding solid lines moving away from this case correspond to $r_-=0.46$, 0.42, 0.38, 0.3, and succeeding dashed lines correspond to $r_+=0.46$, 0.42, 0.38, 0.3. The unstable branch terminates on the neutral branch only over the range $0.4019<r_-<0.5981$ (compare with the approximate formula given in equation 6.5). The unstable modes over this parameter range are true two-cavity modes. Outside this range, all the unstable branches pass through one of the two 'caustics', $\phi=0$, $\psi=\pi$ or $\phi=\pi$, $\psi=0$. This parameter range corresponds to single-cavity-like modes.

Since $\sqrt{1+\tau^2}\gg 1$, we clearly need $\exp[i(\phi+\psi)]\sim -1$. Let us hence write

$$\Delta=\pi-(\phi+\psi). \tag{6.2}$$

Then (6.1) gives

$$\Delta=2\sin\phi/\sqrt{1+\tau^2}. \tag{6.3}$$

The locus of the neutral branch in the $\phi\psi$ phase diagram is shown in Fig. 2. We note that

$$\left(\frac{d\psi}{d\phi}\right)_{\text{neutral}}=-1-\frac{2\cos\phi}{\sqrt{1+\tau^2}}, \tag{6.4}$$

which is only slightly different from -1. Thus, following the arguments of Section 5.1, a tangent point can be obtained only for

$$1-\frac{2}{\sqrt{1+\tau^2}}\leq\frac{r_+}{r_-}\leq 1+\frac{2}{\sqrt{1+\tau^2}}, \tag{6.5}$$

i.e. only over the range of corotation positions given by

$$|\Delta r|=|r_+-r_-|\leq 1/\sqrt{1+\tau^2}. \tag{6.6}$$

For $|\Delta r|$ lying within this range, the unstable branch will intersect the neutral branch at the tangent point, just as we discussed in Section 5.1. The point of intersection is given by

$$\phi=\cos^{-1}(-\Delta r\sqrt{1+\tau^2}). \tag{6.7}$$

However, unlike the $\tau \ll 1$ case, the unstable branch is no longer described by a straight line in the $\phi\psi$-diagram, but bends as shown in Fig. 2.

A more interesting regime is when $|\Delta r|$ lies outside the range in (6.6). The fact that there is no tangent point available on the neutral branch means that the unstable branch has to do something new. Let us assume $r_+ > r_-$ and take $\Delta r = r_+ - r_- \gg 1/\sqrt{1+\tau^2}$. Since the amplifier is strong, we expect $|\Lambda W|$ to be large. Let us consider the case of negative Λ, with $\exp(-\Lambda W) \gg 1$, which corresponds to a growing mode. Equation (5.1.5) now becomes, with appropriate ordering of terms,

$$\sqrt{1+\tau^2}\,[\exp(\Lambda W r_+ + i\phi) + \exp(\Lambda W r_- - i\psi)] - 1 = 0. \tag{6.8}$$

The imaginary part gives

$$\sin\phi = \exp[-\Lambda W(r_+ - r_-)]\sin\psi. \tag{6.9}$$

Substituting this in the real part and solving we find

$$\Lambda = -\frac{1}{2X_-}\ln(1+\tau^2), \tag{6.10}$$

$$\sin\phi = (1+\tau^2)^{\Delta r/2r_-}\sin\psi. \tag{6.11}$$

Note the surprising result that the growth rate is identical to that obtained in equation (4.5) for the single-wall case. Note, in particular, that the growth depends only on $Wr_- = X_-$ and not on X_+ at all. What this means is that the moment the lengths of the two cavities become even slighty unequal, the shorter cavity takes command of the mode, and the second cavity becomes irrelevant. The reason is that the mode in the short cavity grows so strongly during a sound-crossing time of the long cavity that the feedback in the latter is of no consequence at all.

By assuming $\exp(\Lambda W) \gg 1$, we obtain a second solution to equation (5.15) with

$$\Lambda = +\frac{1}{2X_-}\ln(1+\tau^2). \tag{6.12}$$

This is just the complex conjugate of the growing solution given in (6.10), (6.11), and corresponds to the decaying unphysical solution of the single-wall problem discussed at the end of Section 4, involving an incoming wave in the long cavity.

An interesting point is that all the unstable branches in the 'single-wall' regime go through the point $\phi = \pi$, $\psi = 0$ (the corresponding point would be $\phi = 0$, $\psi = \pi$ when $r_- > r_+$). This produces another neat solution of the 'conservation of modes' problem, alluded to in Section 5.1. The fact is that the point $\phi = 0$, $\psi = \pi$ is an inflexion point in the $\phi\psi$-plane of both the neutral and unstable branches. Let us now consider a series of W values, just as we did in the discussion in Section 5.1. Since there is no tangent point in either the neutral or unstable curve, therefore for each value of W, there are neutral as well as growing/decaying modes (one should think of Fig. 6.1 periodically continued along ϕ and ψ). A little thought reveals that the total number of modes is the same in this regime as in the regime where there is a tangent point.

Because of the strong growth rate when $\tau \gg 1$, the mode is dominated in each cavity by the outgoing wave, namely $E(X)$ for $X > 0$ and $E^*(-X)$ for $X < 0$. The amplitudes of these waves are given by (5.1.22) and (5.1.23) (which are valid for any τ), with E and E^* given by (3.1)–(3.4). Thus the dominant waves are $\tau \exp(\frac{1}{2}\Lambda X)$ for $X > 0$ and $\sqrt{1+\tau^2}\exp(\frac{1}{2}\Lambda|X|)$ for $X < 0$. Therefore, provided the cavities are much longer than $1/\Lambda$, the integrated action in the two cavities are equal in magnitude to leading order in $1/\tau$. in fact, a more careful analysis shows that the unstable modes have zero net action to all orders in $1/\tau$.

7 The corotation resonance

Up to this point, we have discussed a very simple system, the 'shearing sheet', in which the properties of the background (Σ, c, A, B, and Ω) are constant. We believe that the qualitative results obtained for this system are applicable to more complicated flows. The shearing sheet, however, does not display one important general phenomenon that is present in almost any other flow, namely, the absorption of action (or more generally energy and angular momentum) at corotation. The corotation resonance deserves a more extensive discussion than this section provides, but we feel it would be misleading to ignore the topic entirely in a paper on general aspects of the stability of differentially rotating flows.

We begin our discussion by deriving a differential equation in Section 7.1 to describe a general flow with non-constant Σ, c, A, B. We use this equation in Section 7.2 to show that the corotation resonance can cause growth or decay of a mode that would otherwise be neutral. However, as we argue in Section 7.3, non-linear effects end growth of such modes at very small amplitudes whenever the tunnelling amplitude τ through the forbidden region is small. [The tunnelling amplitude τ was originally defined in equation (3.12) for the parabolic cylinder equation. We use the same symbol for the tunnelling amplitude in the general case (7.1.8) below.]

The production of growing modes by the corotation resonance has been emphasized recently in PPIII. Their discussion of the role of the resonance is somewhat more detailed than ours; however, they consider only the linear regime and therefore neglect the effect of saturation, which we believe is likely to occur at small amplitudes for resonance-driven modes of this sort (Section 7.3).

7.1 THE GENERAL V EQUATION

The exact (i.e. not linearized) Euler equation for a two-dimensional isentropic fluid in a rotating frame is given in equation (2.1). For a polytropic fluid with an equation of state of the form

$$P=K\Sigma^{\gamma}, \tag{7.1.1}$$

the enthalpy can be written as

$$Q\equiv \frac{\gamma P}{(\gamma-1)\Sigma} \propto \Sigma^{\gamma-1}. \tag{7.1.2}$$

In a general flow, A, B, and Σ depend on x (though Ω is constant, since it is just the angular velocity of our chosen reference frame). Consequently, the specific vorticity ζ (equation 2.7) varies across the flow. In contrast, every fluid element in the shearing sheet has the same specific vorticity ζ_0, and this accounts for the absence of the corotation resonance in that special case.

The linearized form of the vorticity conservation equation is given in (2.23). Combining this equation with (2.21), which remains valid in the general case, we solve for u and Σ':

$$u=-\frac{i}{G}\left(c^2k\frac{dv}{dx}-2B\sigma v\right), \tag{7.1.3}$$

$$\frac{\Sigma'}{\Sigma}=\frac{1}{G}\left[2B\frac{dv}{dx}+\left(k\sigma-\Sigma\frac{d\zeta}{dx}\right)v\right], \tag{7.1.4}$$

where

$$G(x)\equiv 4B^2+c^2k^2-\frac{c^2k\Sigma}{\sigma}\frac{d\zeta}{dx}, \tag{7.1.5}$$

and the sound speed c is given by

$$c^2 = dP/d\Sigma = \gamma K \Sigma^{\gamma-1}. \tag{7.1.6}$$

Substituting these expressions for u, Σ' and c^2 into the perturbed continuity equation, which in the general case is

$$-i\sigma \frac{\Sigma'}{\Sigma} + \frac{u}{\Sigma}\frac{d\Sigma}{dx} + \frac{du}{dx} + iky = 0, \tag{7.1.7}$$

we have the desired equation for v:

$$\frac{d^2v}{dx^2} + \left(\gamma \frac{d\ln\Sigma}{dx} - \frac{d\ln G}{dx}\right)\frac{dv}{dx} + \left(\frac{\sigma^2-\varkappa^2}{c^2} - k^2 + \frac{k\Sigma}{\sigma}\frac{d\zeta}{dx} + \frac{2B\sigma}{c^2k}\frac{d\ln G}{dx} - \frac{4\sigma}{c^2k}\frac{dB}{dx}\right)v = 0. \tag{7.1.8}$$

The coefficients of dv/dx and v in this equation are singular at corotation, which is defined by the condition $\sigma=0$. (As defined here, an unstable mode has a complex corotation radius.) There are also apparent singularities at points where $G=0$, but these are removable in the sense that all solutions for v are regular at such points. This can be demonstrated by the method of Frobenius or, more easily, by writing down the corresponding second-order equations for u and Σ'. The coefficient functions in the latter equations are regular at points where $G=0$, and the expressions for v in terms of u and du/dx or Σ' and $d\Sigma'/dx$ are also regular there. On the other hand, the equation for u has removable singularities where $\sigma^2=c^2k^2$, and the equation for Σ' has removable singularities where $\sigma^2=\varkappa^2$; but these are obviously regular points for the v equation. All three equations do have singularities where $\sigma=0$, and this *corotation singularity* is not removable. (A similar situation occurs in a thick torus, as discussed in Paper I.) The advantage of the v equation is that even its spurious singularities disappear in the shearing sheet, where G is constant. This facilitates the perturbative calculation of the next section.

Corotation is a branch point for all of the perturbed fluid variables. This means that the results

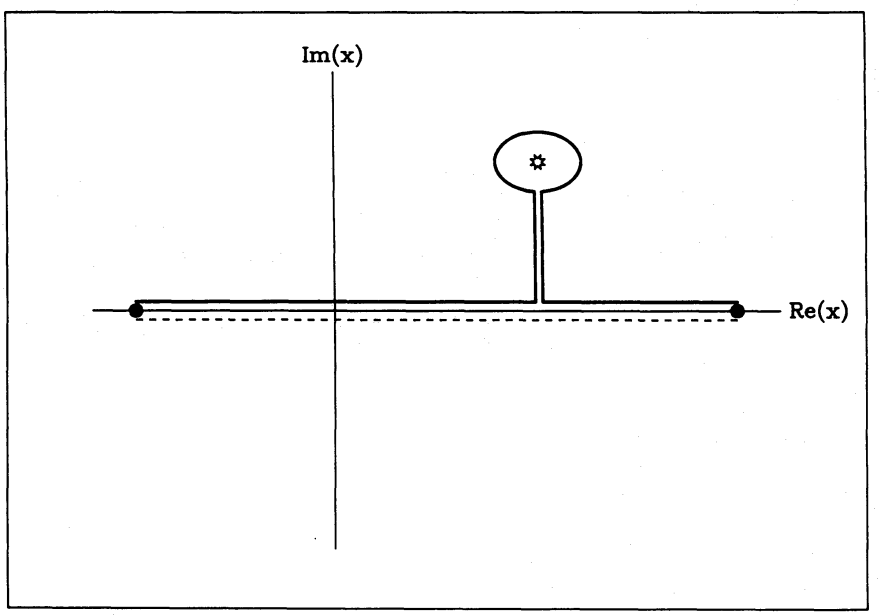

Figure 3. Schematic of integration contour in the complex x plane to be used in searching for eigenmodes of equation (7.1.8) in the presence of a non-zero gradient of specific vorticity. Filled circles indicate boundaries, star marks corotation (shown where it might appear for a strongly decaying mode). Solid curve is a physically acceptable contour for this corotation, dashed leads to an unphysical mode not corresponding to the solution of an initial value problem.

found for v and ω will depend upon the path of integration in the complex x plane. [It is convenient to require that $B(x)$ and $\Sigma(x)$ be analytic.] All paths must begin and end on the real axis, at the left- and right-hand boundaries; but the $[v(x), \omega]$ pairs determined along paths passing below corotation generally cannot be analytically continued into those determined along paths passing above corotation (see Fig. 3). Which is the correct choice?

The answer has been given by Lin (1955). Briefly, the eigenfrequencies ω that we seek are the positions of poles in the integrand of an inverse Laplace transform giving $v(x, t)$ at $t>t_0$ in terms of $v(x, t_0)$; that is, we seek modes that correspond to the solution of some initial value problem. The inverse transform is to be carried out along a path in the ω plane at sufficiently large Im (ω) as to pass above all such poles or other possible singularities; or along any other path that is equivalent to this by analytic continuation. We carry out this analytic continuation by ensuring that the contour in the x plane always lies on the same side of corotation as it would if ω had a large positive imaginary part. This translates to the requirement that the path should pass *above* the complex corotation x_c. (In general there will be more than one solution to the equation, $V(x_c)=\omega/k$, that solves for the complex corotation point x_c. But in this paper we shall consider only cases in which $V(x)$ is approximately or exactly equal to $2Ax$, with A a negative constant; then there is a one-to-one correspondence between x_c and ω for a given k.)

7.2 GROWTH RATES FROM FIRST-ORDER PERTURBATION THEORY

In understanding the effects of the corotation resonance, it is very instructive to consider the limit in which the resonance is weak enough that it can be treated as a perturbation, although a singular one. Thus we begin with a neutral mode (v_0, ω_0) of the shearing sheet ($\zeta=\zeta_0$=constant). Then ω_0 is of course real and so is the corotation radius x_c. We shall estimate the imaginary part of ω to first order in $d\zeta/dx$. Using subscripts 0 and 1 to denote the zeroth and first-order terms in an expansion in powers of $d\zeta/dx$, we write $\omega=\omega_0+\omega_1$, and $v=v_0+v_1$. The differential equation for v_1 then takes the form

$$\frac{d^2v_1}{dx^2}+\left(\frac{\sigma_0^2-\varkappa_0^2}{c_0^2}\right)v_1=RHS, \tag{7.2.1}$$

where RHS involves terms proportional to v_0 or dv_0/dx multiplied by ω_1 or $d\zeta/dx$. The homogeneous form of (7.2.1) in which $RHS \to 0$ has linearly independent solutions v_0 and $\bar{v}_0$, where only the first satisfies the boundary conditions. The inhomogeneous form therefore has the solution

$$v_1(x)=v_0(x)\int_{x_-}^{x} RHS(x')\,\bar{v}_0(x')\,dx'-\bar{v}_0(x)\int_{x_-}^{x} RHS(x')\,v_0(x')\,dx'. \tag{7.2.2}$$

Here x_- and x_+ are the positions of the left- and right-hand boundaries.

For simplicity, we will assume that the boundary condition is not $u=0$ but rather $v=0$ or $dv/dx=0$. Then v_0 and v_1 must satisfy the same condition separately, and therefore the second integral in (7.2.2) must vanish. Explicitly, this gives

$$\omega_1\left(\frac{2}{c^2}\int_{x_-}^{x_+}\sigma_0\,|\,v_0\,|^2\,dx\right)=-\int_{x_-}^{x_+}\left(\frac{k\Sigma}{\sigma}\frac{d\zeta}{dx}+\frac{2B\sigma}{c^2k}\frac{d\ln G}{dx}\right)+\text{real terms}, \tag{7.2.3}$$

where the omitted 'real terms' are non-singular and therefore do not contribute to the imaginary part of ω_1, which is proportional to $-i\pi$ times the sum of the residues at $x_{c,0}$ of the terms retained. (The choice of the factor $-i\pi$ is because we pass *above* the pole from left to right, in accordance

with the prescription discussed above.) Thus we find

$$\mathrm{Im}\,(\omega_1)=\frac{\pi\Sigma c^4}{2A(4B^2+c^2k^2)}\left(\frac{dv_0}{dx}\right)^2\frac{d\zeta}{dx}\bigg|_{x=x_c}\Big/\int\sigma_0(x')\mid v_0(x')\mid^2 dx'. \tag{7.2.4}$$

The point of this exercise is that equation (7.2.4) has a simple interpretation. The integral in the denominator is like the total action of the original neutral mode. The numerator on the other hand is determined by flow properties that are local to corotation. This term is proportional to $d\zeta/dx$, and can be interpreted as the rate of absorption of action by the resonance. Hence (7.2.4) says that the rate of growth or decay of the mode is the rate of absorption of action at corotation divided by the total action of the mode. If the sign of the action absorbed is the same as the sign of the net action of the mode, then the mode decays; if the signs are opposite, the mode grows. Apart from its dependence on $d\zeta/dx$, the rate (7.2.4) is of order τ, since at corotation, in the middle of the forbidden region, v is of order $\sqrt{\tau}$ compared to its amplitude in the permitted region. Thus, Im (ω_1) is in principle of the same order as the growth rate (5.1.21) of balanced modes in the shearing sheet. In practice we find that the growth rate implied by, (7.2.4) tends to be somewhat smaller than that of balanced modes with comparable τ.

A more physical way of understanding the absorption at corotation is to consider the forces exerted on individual fluid elements by a pattern of pressure perturbations that vary as exp $(iky-i\omega t)$, with ω being real. We shall not go into the mathematical details, which are somewhat lengthy, but we shall briefly sketch this viewpoint because it is the basis of our remarks on saturation in Section 7.3. A detailed treatment has been given by Lynden-Bell & Kalnajs (1972) in a stellar-dynamical context, and the physics is closely analogous to linear Landau damping in a plasma (Lifshitz & Pitaevskii 1981).

Away from corotation, fluid elements feel a periodic force along y as they ride over the hills and valleys of the pressure perturbation. Therefore they experience no secular change in energy or angular momentum. Very close to corotation, however, fluid elements feel forces acting in the same direction for a very long time (in the linear theory). Even so there is no net absorption by the fluid in first order when we average along y, since for every fluid element on the uphill side of the pressure perturbation there is another on the downhill side. In second order however there is an effect. When subjected to a steady force per unit mass F along y, a fluid element gains angular momentum at a steady rate and will move along x at the rate $\dot{x}=F/2B$. Thus when $B>0$ (the usual case), a particle just inside corotation subjected to a positive F will move out toward corotation and slow down, prolonging the time it spends on the downhill slope, whereas its companion on the uphill slope at the same original x will move inward and speed up. Hence at x infinitesimally less than x_c, there is a net tendency in second order for the fluid to absorb angular momentum. The reverse is true on the other side of corotation. If one then integrates over x, the result is that the total rate of absorption of angular momentum depends on the relative amounts of matter on each side of corotation and on the variation in B. In fact the decisive quantity works out to be precisely the gradient in B/Σ, i.e. the gradient of the specific vorticity.

When Im (ω) is finite, the absorption occurs over a region of width $\sim$Im $(\omega)/\mid 2Ak \mid$ in x centred on x_c.

7.3 NON-LINEAR SATURATION OF THE COROTATION RESONANCE

In this subsection we are concerned with growing modes only.

Both of the methods outlined in Section 7.2 for calculating the absorption at corotation assume that fluid particles deviate from their positions in the unperturbed flow by distances $\Delta y \ll 1/k$. This ceases to be true when the mode reaches a sufficiently large amplitude. Consider a particle whose unperturbed position would be exactly at corotation with azimuthal phase y_0. Then,

schematically,

$$\frac{d^2\Delta y}{dt^2} = -a_0 \cos\,[k(\Delta y + y_0)]. \tag{7.3.1}$$

The coefficient a_0 is linearly proportional to the amplitude of the mode at corotation, because it arises from gradients in the perturbed pressure. Therefore a_0 has the exponential growth rate $+\mathrm{Im}\,(\omega)$; but if we could neglect the time dependence of a_0, then (7.3.1) would be like the familiar pendulum equation and Δy would oscillate with a frequency of order

$$\omega_s \equiv \sqrt{ka_0}. \tag{7.3.2}$$

When the amplitude of the mode is large enough so that $\omega_s > \mathrm{Im}\,(\omega)$, Δy will oscillate repeatedly over a typical distance $\sim 1/k$ during a single e-folding of a_0. The sign of the torque on this fluid element will change twice in every oscillation, and the angular momentum of the element will no longer show a secular change. Since the growth of the mode depends upon the corotation absorption, at this point the mode will saturate. This is what we mean by saturation of the resonance and it is directly analogous to non-linear Landau damping in a plasma.

The acceleration a_0 of particles at corotation is determined mainly by the y-pressure gradient, which is proportional to $k\Sigma'$. Since $\sigma = 0$, we find from equation (2.25) that this quantity is proportional to dv/dx. Thus, by setting $\omega_s = \mathrm{Im}\,(\omega)$, we find

$$\frac{dv^{\mathrm{sat}}}{dx}(x_c) \propto a_0^{\mathrm{sat}} \approx \frac{[\mathrm{Im}\,(\omega)]^2}{k}. \tag{7.3.3}$$

But the amplitude of v at corotation is of order $\sqrt{\tau}$ times the amplitude of v in the permitted region, and as shown in Section 7.2, $\mathrm{Im}\,(\omega) \propto \tau$. Therefore, the limiting amplitude in the permitted region is

$$v^{\mathrm{sat}}(\text{permitted}) \propto \tau^{3/2}. \tag{7.3.4}$$

Usually $\tau \ll 1$, so that the limit (7.3.4) is severe. As remarked in Section 6, however, a self-gravitating disc can have $\tau \gg 1$, and in fact most of the growing modes calculated for models of spiral galaxies appear to be of the type discussed in this section: the action is concentrated on one side of corotation (usually, but not always, on the inside), and the growth appears to depend on a strongly absorbing corotation resonance (see Toomre 1981, and references therein).

The limit (7.3.4) applies only to resonance-driven growing modes. It does not apply to balanced modes, which owe their growth to feedback and could have saturation amplitudes of order unity.

8 Numerical examples

The object of this section is to support the analytical discussions of the previous sections with concrete numerical examples. For convenience, the units $c = -2A = 1$ will be used. Unless otherwise stated, the boundary condition is $u = 0$ at $x_b = \pm 5$. The Mach number, M, of the shear from the centre of the flow to either edge is thus 5.

8.1 METHOD

All results for the shearing sheet follow from the known properties of the Parabolic Cylinder functions in the complex plane (Abramowitz & Stegun 1972). However, it is more convenient to integrate equation (2.26) numerically, because this can be done accurately and quickly, and

because we shall later generalize the equation to non-constant velocity and surface-density profiles.

Eigenvalues ω (or equivalently, complex corotations $x_c=-\omega/k$) of equation (2.26) were determined by the shooting method. Instead of shooting from one boundary to the other, we chose a tentative value for the complex corotation x_c, and used that as a starting point, integrating from there to the two boundaries. For given values of x_c and k, the values of u at the two boundaries are linear functions of v and dv/dx at x_c, and the 2×2 matrix $\mathbf{E}$ expressing these functions was determined by four numerical integrations. The boundary condition $u=0$ requires the determinant of $\mathbf{E}$ to vanish. Therefore, the dispersion relation given x_c as a (multiple-valued) function of k or *vice versa* is defined implicitly by

$$\det \mathbf{E}(x_c, k; x_0)=0. \tag{8.1.1}$$

This equation was solved numerically by the Newton–Raphson Method. When the iterations converged to an (x_c, k) pair satisfying (8.1), we could then easily reconstruct the corresponding eigenmode, $v(x)$. An efficient, high-order method (the Bulirsch–Stoer scheme – *cf.* Press *et al.* 1986) was used for all of the integrations. We demanded that k be real, but then x_c could be complex.

As discussed in Section 7, corotation is a singular point of the equations when the unperturbed specific vorticity has a non-vanishing gradient there. In this case, the physical eigenmodes can be found by integrating along a contour that passes *above* corotation in the complex x_c-plane. Accordingly, we took the starting point of the integration to be x_c+i at each iteration.

8.2 WKB MODES AND PHASE CONDITIONS

Fig. 4 shows part of the dispersion relation for the neutral modes when $B=0$. The solid lines are the neutral curves, corresponding to the numerically determined loci of real corotations x_c as a

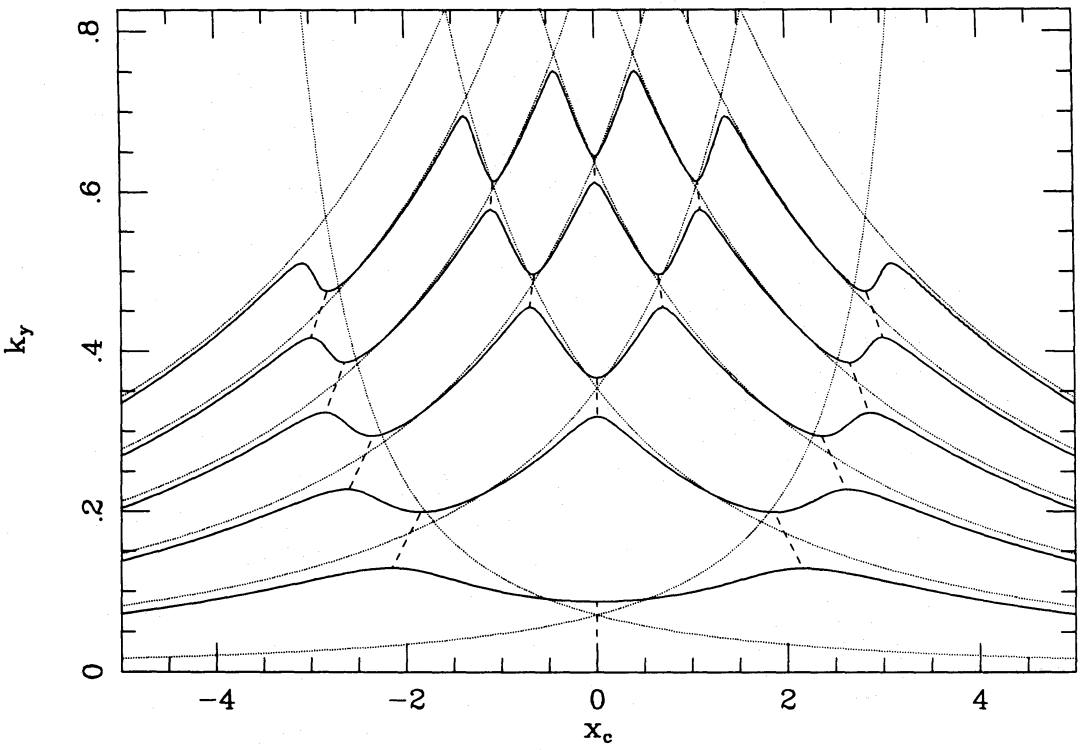

Figure 4. Dispersion plot for $B=0$. Solid lines: numerically calculated curves corresponding to neutral modes. Dashed lines: numerically calculated curves for unstable modes. Dotted lines: WKB curves from equation (8.2.1).

function of the wave-vector k. Unstable modes have complex corotations and are shown by dashed lines. A complex branch begins at each local maximum of the neutral curves and extends to the nearest minimum of the next curve up. Thus as k increases, two neighbouring neutral modes merge to form a complex-conjugate pair; and at still larger k that pair recombines and divides into two neutral modes again. The total number of real and complex modes in the diagram, i.e. the number of solutions for x_c, changes as a function of k only because new branches enter from the region $|x_c|>5$, 'outside' the shearing sheet. The newly arriving modes are always neutral when they first appear because, as discussed in Section 3, only modes with corotation inside the fluid can grow or decay.

The entire diagram could be reflected about the horizontal $k=0$ axis, since for every mode with positive k there is an equivalent mode with negative k. Consequently, there is a complex branch connecting the minimum of the lowest-lying neutral curve to the maximum of its mirror image at $k<0$. This is the *principal branch*, which was discussed in Section 5.2 and to which we shall return below in Section 8.3. Fig. 4 has an obvious reflection symmetry about the line $\mathrm{Re}\,(x_c)=0$ as well, which is a consequence of the left–right symmetry of the system.

A comparison of Fig. 4 with Fig. 5 of Paper I shows a remarkable qualitative similarity. The system studied there was a three-dimensional incompressible torus, and at first it may seem surprising that the two-dimensional shearing sheet should simulate that system so well. The point is that the 'principal branch' in the torus behaves like a two-dimensional system to a very high precision, while the higher-order WKB modes behave like *surface disturbances*, and are again essentially two-dimensional. It is thus quite natural for the torus and the shearing sheet to be so similar.

We showed in Section 5.1 that the two cavities between corotation and the walls of the shearing sheet have a crucial influence on the nature of the modes. A mode is obtained only when at least one of these cavities is resonant. When a single cavity is resonant, we have a neutral mode, and when both cavities are resonant, we have a pair of growing and decaying modes. The dotted curves in Fig. 4 illustrate these points. These curves show the WKB phase conditions corresponding to the two cavities being resonant. Each curve begins at one boundary and rises monotonically to higher values of k as x_c moves toward the other boundary, diverging toward infinite k. The curves issuing from the left-hand edge express the condition that an n-noded WKB eigenfunction fit into the permitted region between corotation (actually the turning point on the right of corotation) and the right-hand wall. Each such curve has a mirror-image twin giving the condition for the dual eigenfunction that lives between corotation and the left-hand wall. Counting from the bottom up at the left-hand edge, the curves correspond to 0, 1, 2, . . . , 5 nodes on the right of corotation.

In the interests of improving the agreement between the WKB results and the neutral curves, we have been rather careful about the constants in the phase condition. In the discussion in Sections 4 and 5, we assumed a very simple boundary condition and replaced the true WKB conditions by $\phi=2n\pi$ for a resonant right-hand cavity, and $\psi=2n\pi$ for a resonant left-hand cavity. However, in calculating the dotted curves in Fig. 4, we have used the precise WKB condition, which takes the form

$$2\int_{x_t}^{x_b} k_x\,dx-\frac{\pi}{2}+2\arctan\left(\frac{2B\,|x_b-x_c|}{k_x(x=x_b)}\right)=2\pi n,\qquad n=0,1,2,\ldots, \tag{8.2.1}$$

where

$$k_x\equiv+[k^2(x-x_c)^2-k^2-\varkappa^2]^{1/2} \tag{8.2.2}$$

is the WKB wavenumber derived from (2.26), x_t is either of the two *turning points* [the solutions of $k_x(x_t)=0$], and x_b is the boundary on the same side of corotation as x_t. The term $\pi/2$ in (8.2.1) is

the standard phase shift produced at a simple turning point when the tunnelling through the forbidden region is neglected. The arctangent term is the phase shift acquired in reflecting from the boundary; it is determined straightforwardly by inserting the lowest-order WKB wavefunction into the boundary condition, $u=0$ (equation 2.24). For $B=0$, the latter phase shift vanishes because $dv/dx=0$ at the boundary, and so the reflected wave is in fact the geometrical reflection of the incident wave.

For the parameters of Fig. 4, the tunnelling amplitude τ defined in equation (3.12) is not small (in fact $C=k/2$), so WKB cannot be expected to be very accurate, especially in the lower parts of the diagram. Nevertheless, the agreement between the solid and dotted curves is generally impressive. Also, the phase conditions intersect in the gaps between neutral curves where the complex branches lie, as expected from the analysis of Section 5.1. Thus each complex branch can be identified uniquely by the notation (n_l, n_r), where the integers n_l *and* n_r are the numbers of nodes on the left and right of corotation. In this classification scheme, the principal branch is (0, 0).

The case $B=0$, $M=5$ shown in Fig. 4 corresponds to fairly large τ and therefore gives large and easily visible gaps, and growth rates that are relatively strong (see equation 5.1.17). The fastest growth rate is 0.09644 and occurs on the principal branch (the unit of frequency is $q\Omega$ since $2A$ has been set to -1). A growth of 0.089 is found in the (1, 0) gap. The diagram for $B=0$ but $M=2$ (not shown) has much smaller gaps. This is because the lowest-lying neutral curves occur at ks that are larger by roughly $(5/2)^2$, and so the Cs are larger and the tunnelling amplitudes τ are much smaller.

Fig. 5 shows another case of interest, the 'Keplerian' case, $q=3/2$, $B=1/6$. The gaps between the neutral curves are obviously much narrower than in Fig. 4 and the agreement between the WKB predictions and the numerically computed neutral curves is much better. Both of these effects are consequences of smaller τ. More significantly, the principal branch has disappeared.

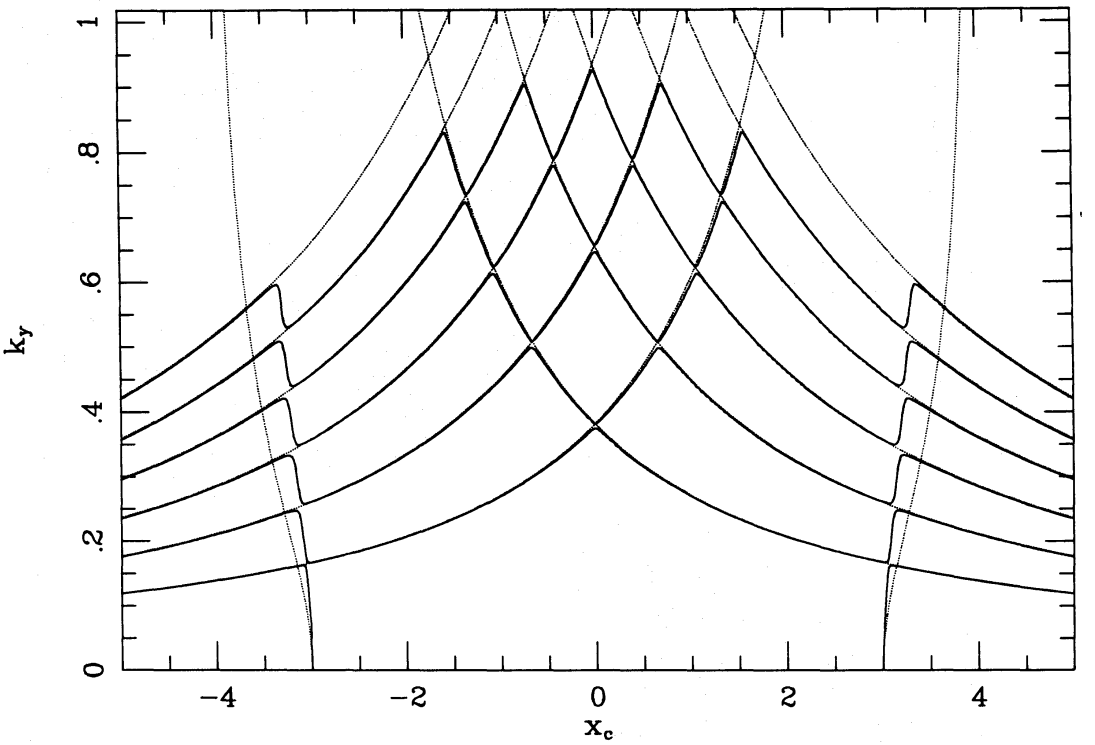

Figure 5. As in Fig. 4, but for $B/(-2A)=1/6$. Near-vertical dotted curves are from equation (B.3), all other dotted curves are from equation (8.2.1).

Setting $\Lambda=0$ and $M=5$ in equation (5.2.13), we see that the minimum q down to which the principal branch survives is $q_{\min}\approx 1.889$, whence the largest B for which the principal branch exists at this Mach number is 0.0294.

The $n=0$ WKB phase curve is not shown in Fig. 5; in fact, there appear to be no solutions to (8.2.1) with $n=0$ for $k<0.763$ (approximately). The $n=0$ curve has been replaced by a nearly vertical dotted curve that is discussed in Appendix B. The other dotted curves are, from bottom to top, $n=1$ through 6. Also of interest in Fig. 5 are the nearly vertical notches in the neutral curves near the boundaries. These are the signature of edge modes, and we defer further discussion of them to Section 8.3 and Appendix B.

Fig. 6 shows the eigenfunctions corresponding to three modes near the (3, 1) gap in Fig. 5. The first two lie on the neutral curve just below the gap and to either side of it, while the third is a complex mode in the middle of the gap. It is clear that the two neutral modes (Figs 6a, b) are *unbalanced*, since most of their action (energy or momentum) lies on one side of corotation. (However, the amplitude on the subdominant side is not very small because the tunnelling amplitude is substantial, $\tau\approx 0.122$.)

In Fig. 7 we have plotted the action density, ϱ_*, and the flux, j_*, defined in equations (3.8) and (3.10), for the complex mode of Fig. 6c. We see that the action density is positive for $x>x_c$ and negative for $x<x_c$, as expected. Numerical integration reveals that the positive and negative actions cancel exactly, so that the mode has zero net action. The mode is thus *balanced*. This is true for every unstable mode of the shearing sheet, whether growing or decaying.

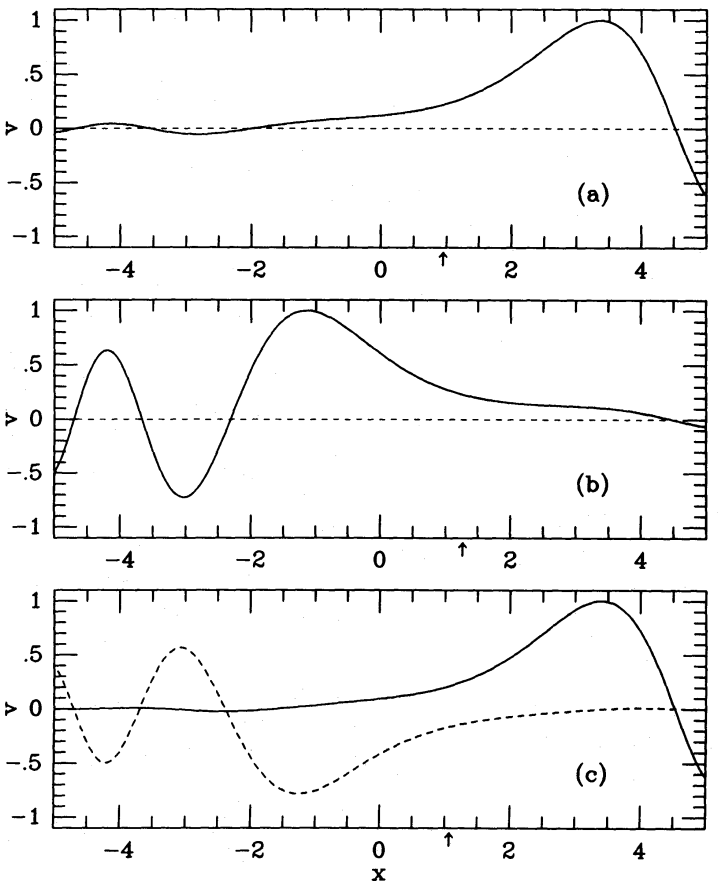

Figure 6. Modes near the (3, 1) gap of Fig. 5. The solid lines show Re (v) and the dashed lines show Im (v) of the eigenfunctions. Small arrows on the abscissa mark (real part of) corotation. (a) $k=0.58$, $x_c=0.9459$ (neutral mode); (b) $k=0.58$, $x_c=1.2634$ (neutral mode); (c) $k=0.6194$, $x_c=1.0672-i0.0214$ (growing mode).

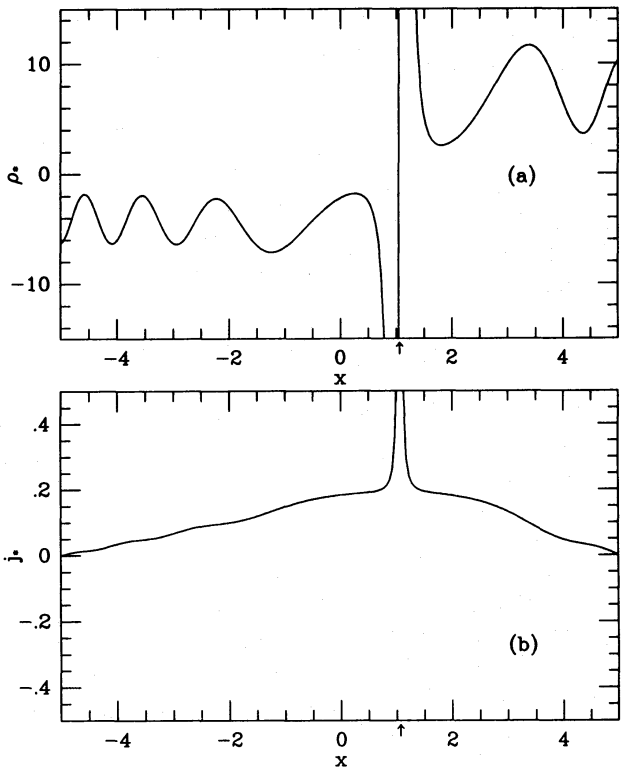

Figure 7. (a) Action density ϱ_* of the mode shown in Fig. 6c. (b) Flux j_* of the same mode.

We note that both ϱ_* and j_* in Fig. 7 have singularities at corotation. This is because these quantities have been defined in a Lagrangian sense. Fluid elements in the vicinity of corotation move at the same speed as the pattern and undergo the same sense of acceleration for a long time, building up large displacements as time goes on. In a Eulerian sense, however, the perturbations are non-singular, and one might suspect that a Eulerian action density may be more suitable for our analysis. Unfortunately, as we discuss in Appendix A, we have been unable to find a Eulerian action density that satisfies all our requirements.

8.3 THE PRINCIPAL BRANCH AND EDGE MODES

When the principal branch exists, it extends down to $k=0$. Although the growth rate $\mathrm{Im}(\omega)$ vanishes at $k=0$, the corotation x_c is still complex because $\mathrm{Im}(\omega)\approx k\,\mathrm{Im}[x_c(k=0)]$. We therefore speak of the $k=0$ modes as 'growing' or 'decaying', even though they are technically neutral. The $k=0$ modes are of course not equivalent to any axisymmetric neutral modes (the latter do not have a finite corotation point), and could not be realized in a finite system, where the possible values of k would be discrete. They are best understood as idealized limits of sequences of small-k modes, and so we shall use the notation $k=0^+$ for them henceforth.

It is useful to begin our examination of the principal branch by studying the $k=0^+$ modes as a function of B. We recall that in this limit the v equation reduces to (5.2.9), or in the units of this section,

$$\frac{d^2v}{dx^2}-\varkappa^2 v=0. \tag{8.4.1}$$

Thus, except when $B=0$, the eigenfunction is evanescent throughout the fluid. Therefore the

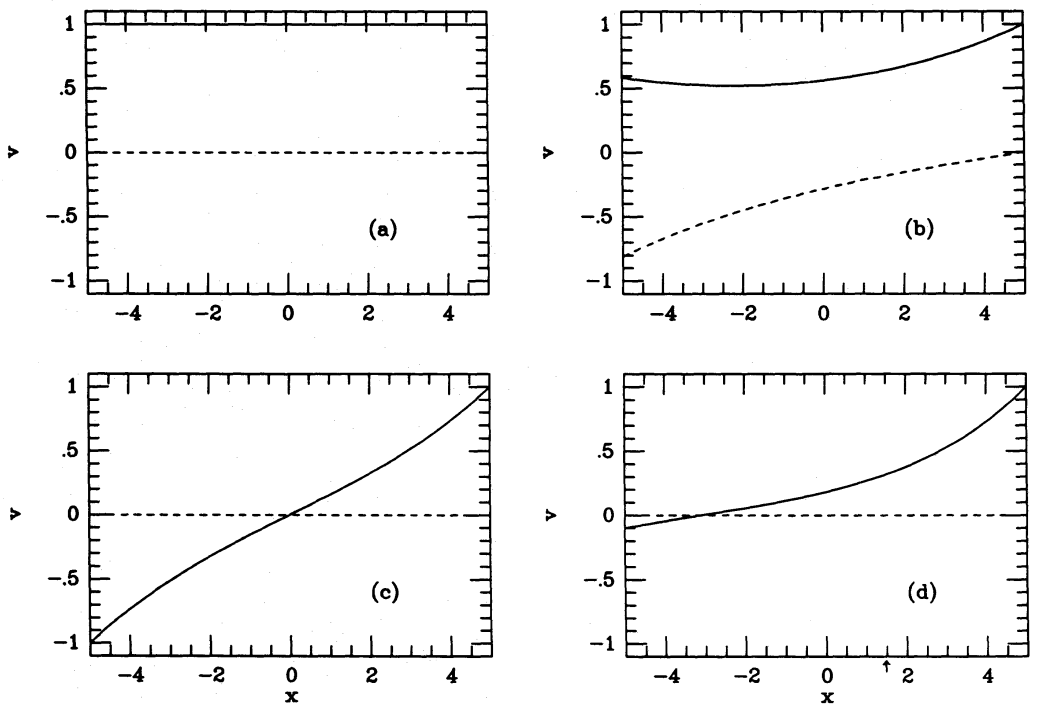

Figure 8. $k=0^+$ eigenfunctions. The solid lines show Re (v) and the dashed lines show Im (v) of the eigenfunctions. (a) $B=0$, $x_c=-i2.707$ (growing mode); (b) $B=0.015$, $x_c=-i1.689$ (growing mode); (c) $B=0.0294546$, $x_c=-i0.00114$ (marginal case between growing and neutral modes); (d) $B=0.045$, $x_c=1.476$ (neutral mode).

$k=0^+$ principal mode is not even approximately describable by the WKB notions underlying equation (8.2.1). The boundary condition (2.23) becomes in the present units

$$\frac{dv}{dx}=2B(x_b-x_c)\,v, \tag{8.4.2}$$

which is correct for all values of k.

Fig. 8 shows the $k=0^+$ eigenfunctions for several values of B. These results were obtained numerically, but in the limit of $k=0$ (or $X_0=0$), the analytical formulae of Section 5.2 are actually exact. Thus, the case shown in Fig. 8a for $B=0$ is given by equation (5.2.5), while the cases in Fig. 8b, c are described by equation (5.2.11). The mode for $B=0$ in Fig. 8a is exceptional in that the eigenfunction is real and symmetric. The motion here corresponds to sausage-like distortions of the fluid. Fig. 8c is the critical case (for this M), $B_{crit}\approx 0.0294546$, $q=q_{min}\approx 1.88874$, in which the principal branch is just vanishing and $\mathrm{Im}\,(x_c)\to 0$. The eigenfunction is again real, but it is antisymmetrical around corotation. In this case, the motion corresponds to kink-distortions of the fluid. For B larger than the above critical value, the $k=0^+$ modes are truly neutral. Fig. 8d gives an example; there is of course a mirror-image twin for this mode. Thus as B passes $B_{crit}(M)$, the growing and decaying $k=0^+$ modes combine and immediately divide into a pair of neutral modes, each of which hugs one of the boundaries. As B continues to increase, the neutral modes evolve into eigenfunctions that live near either wall, and whose amplitudes decrease exponentially to very small values toward the opposing wall.

The nearly vertical dotted curves in Fig. 5 are a WKB approximation for these wall-hugging modes, but they are not based on equation (8.2.1), which is appropriate only for modes whose action is predominantly in the permitted region. As we have just seen, the modes that connect continuously to $k=0^+$ store their action mostly or entirely in the forbidden region if $B>0$.

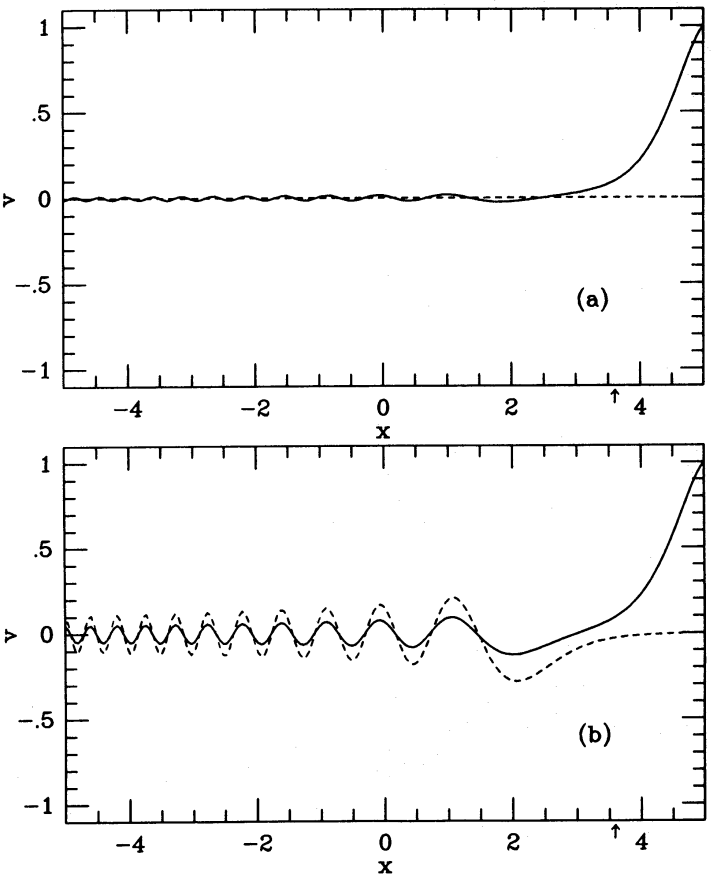

Figure 9. Edge modes for $B/(-2A)=1/6$ (the 'Keplerian' case). The solid lines show Re (v) and the dashed lines show Im (v) of the eigenfunctions. (a) A neutral mode with $k=2$, $x_c=3.601$. (b) A growing mode with $k=1.9$, $x_c=3.589-i0.0033$, and growth rate 6.215×10^{-3}.

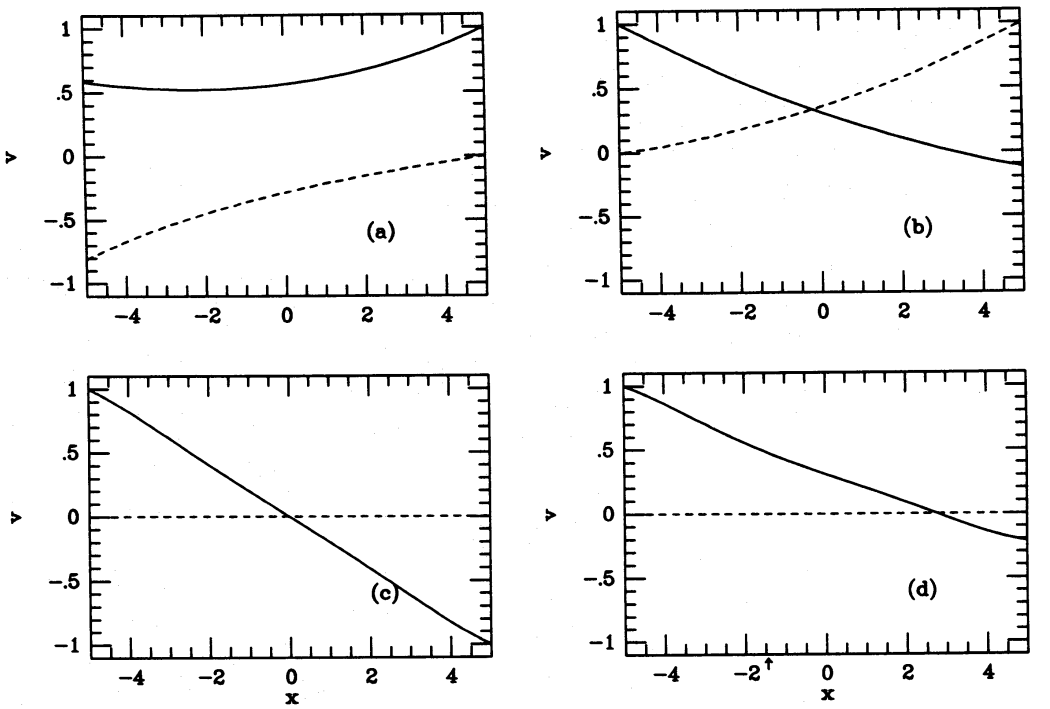

Figure 10. Modes on the principal branch for $B/(-2A)=0.015$. The solid lines show Re (v) and the dashed lines show Im (v) of the eigenfunctions. (a) $k=0$, $x_c=-i1.689$ (same as in Fig. 8b); (b) $k=0.0445$, $x_c=-i1.135$ (maximum growth for this value of B); (c) $k=0.0656675$, $x_c=-i0.0162$ (marginal case between growing and neutral modes); (d) $k=0.1$, $x_c=-1.4538$ (neutral mode).

Appendix B derives an approximate formula (equation B.3) to describe the dispersion curve of this mode.

Equation (5.1.21) predicts that for a given barrier penetration τ, the growth rate is maximized when x_c is as close to one wall as possible. This is confirmed in Fig. 5, as the largest gaps appear where the edge mode intersects one of the other neutral modes. The largest growth of all should occur when C is minimized, i.e. when $k \approx \varkappa$. In Fig. 5, the largest growth is 0.0245 and is found in the (7, 0) and (0, 7) gaps at $k=0.695$, which agrees very well with $\varkappa=2/3$. Fig. 9a and b show a neutral edge mode and a growing mode in one of the edge-mode gaps. Note that most of the action is concentrated in the short cavity between corotation and the wall on the right.

Returning to the principal branch, we see in Fig. 10 a progression of unstable modes at fixed B ($=0.015$) and increasing k. Again, the principal branch terminates in a mode that is antisymmetric around corotation. At still larger k, we find a pair of nodeless neutral edge modes, describable by equation (B.3), whose corotations move towards the two boundaries.

The principal branch of the shearing sheet therefore has many qualitative features in common with that of the narrow torus discussed in Paper I. Both can be interpreted as a pair of coupled edge modes, and both exist only for q larger than some minimum. There are also important differences, however, the most prominent of which is that the principal branch of the torus exists even for a two-dimensionally incompressible fluid (the 'thin ribbon' of Paper I), whereas that of the shearing sheet requires a minimum Mach number across the flow. This difference can be traced to the difference in boundary conditions.

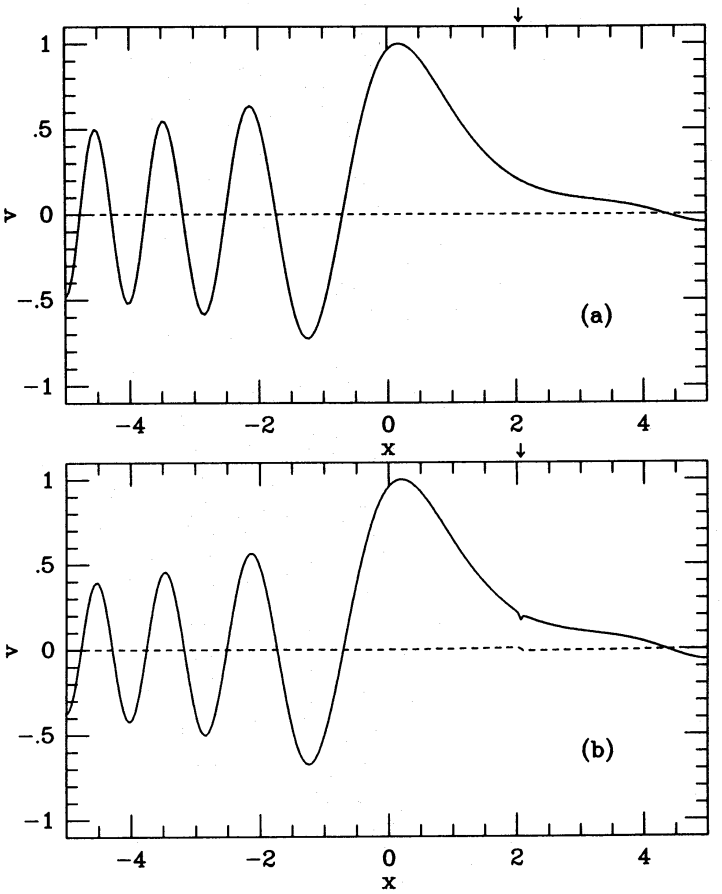

Figure 11. Modes for $B/(-2A)=1/6$, $ck/|2A|=1.0$. The solid lines show Re (v) and the dashed lines show Im (v) of the eigenfunctions. (a) $\alpha \equiv d \ln \Sigma/dx=0$ (no resonance); (b) $\alpha=-0.1$ (resonance-driven unstable mode): note the notch at corotation.

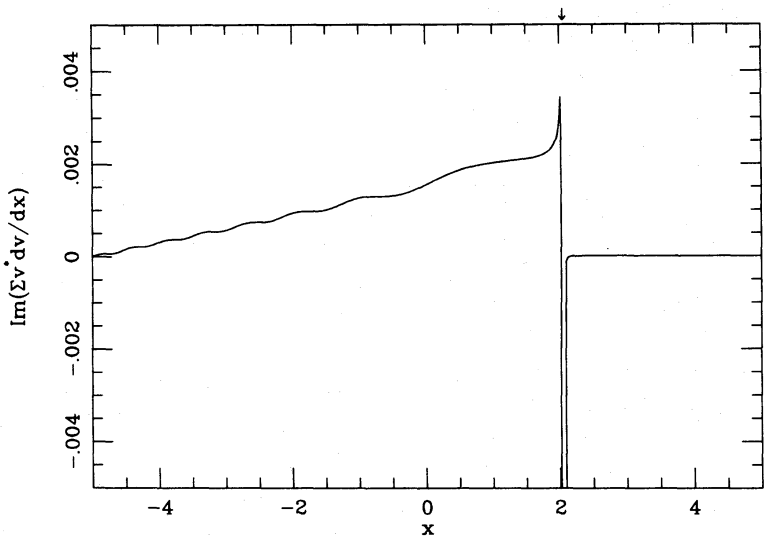

Figure 12. The flux, as defined in equation (A.27), for the mode of Fig. 11b.

8.4 THE COROTATION RESONANCE

We showed in Section 7 that when the specific vorticity ζ varies with x, the equation for v takes the form (7.1.8), which is generally singular at corotation. We used perturbation theory to show that a mode which would otherwise be neutral will grow or decay in the presence of this singularity. For the purposes of illustration, we numerically examine here a simple case in which c, A, Ω (and hence also B) are constant, but

$$\Sigma(x)=\Sigma(0)\exp(\alpha x), \tag{8.5.1}$$

so that $d\zeta/dx \propto -d\ln\Sigma/dx$. We also take $\gamma=1$ in (7.1.1) since otherwise we would have to vary the entropy in order to keep c constant. As in Section 7, the boundary condition in this subsection will be $dv/dx=0$ rather than $u=0$.

Fig. 11a displays a neutral mode of this system for $\alpha=0$, when there is no corotation resonance ($x_c=2.0530$). Fig. 11b shows what happens to this mode when $\alpha=-0.1$: a small kink appears at

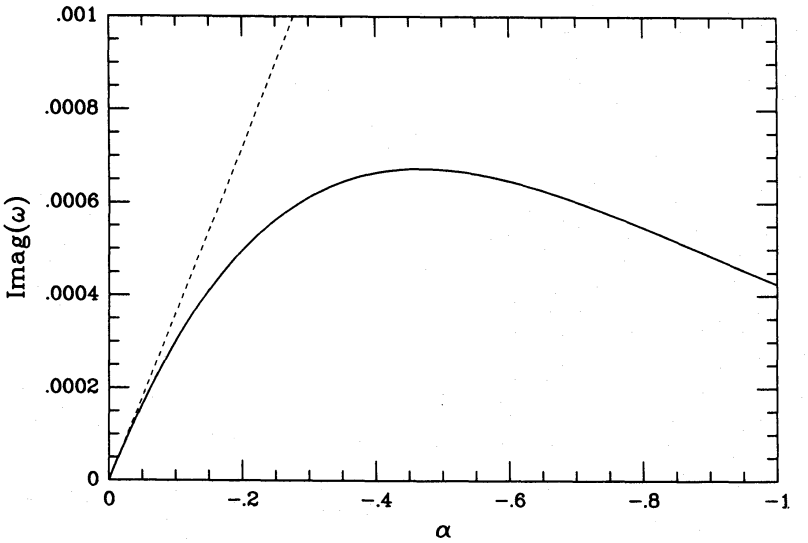

Figure 13. Solid line: growth rate as a function of the strength of the corotation resonance for modes which reduce to that of Fig. 11a when $\alpha=0$. Dashed line: first-order perturbation theory, equation (7.2.4).

corotation, although the mode is not much changed elsewhere. Although it is barely visible in this diagram, the mode has also acquired a small imaginary part. Correspondingly, there is a non-zero flux, which is shown in Fig. 12. Since the boundary condition used in the analysis of Section 7 was not $u=0$, but rather $dv/dx=0$, the appropriate flux is not j_*. We have instead plotted the Eulerian flux, $\mathrm{Re}\,(-i\Sigma v^* dv/dx)$, from equation (A.27). Fig. 12 clearly shows that corotation is emitting negative action and causing this negative-action mode to grow. The fluid to the right of corotation plays no role in this instability.

Fig. 13 compares the actual growth rate with the prediction (7.2.4) of first-order perturbation theory. The perturbative result is accurate for very small α but overestimates the growth rate by almost a factor of 10 when $\alpha=-1$. In fact, the maximum growth rate produced by the corotation resonance is quite small compared to the growth rate of nearby balanced modes in the $\alpha=0$ system. For instance, the largest growth rate in the nearest gap region is $\approx 1.08\times10^{-2}$ [at $k=1.0757$, $\mathrm{Re}\,(x_c)=1.808$].

When $\alpha>0$, the mode decays. This is because corotation now emits positive action, which has the effect of reducing the net negative action of the mode. In this case the actual decay rate *exceeds* the perturbative prediction. In this sense, the corotation resonance is more efficient at producing decay than growth.

Acknowledgments

RN was supported by NSF grant AST-8611121, PG by NSF grant AST-8313725, and JG by a W. M. Keck Foundation grant and by NSF grant PHY-8217352.

References

Abramowitz, M. & Stegun, I. E., 1972. *Handbook of Mathematical Functions,* 10th printing, US Government Printing Office, Washington, D.C.
Blaes, O. M., 1985. *Mon. Not. R. astr. Soc.,* **216,** 553.
Blaes, O. M. & Glatzel, W., 1986. *Mon. Not. R. astr. Soc.,* **220,** 253.
Blandford, R. D., 1976. *Mon. Not. R. astr. Soc.,* **176,** 465.
Blandford, R. D. & Payne, D. G., 1982. *Mon. Not. R. astr. Soc.,* **199,** 883.
Case, K., 1960. *Phys. Fluids,* **3,** 143.
Drazin, P. G. & Reid, W. H., 1981. *Hydrodynamic Stability,* Cambridge University Press, London.
Goldreich, P., Goodman, J. & Narayan, R., 1986. *Mon. Not. R. astr. Soc.,* **221,** 339 (Paper I).
Goldreich, P. & Lynden-Bell, D., 1965. *Mon. Not. R. astr. Soc.,* **130,** 125.
Goldreich, P. & Narayan, R., 1985. *Mon. Not. R. astr. Soc.,* **213,** 7P.
Goldreich, P. & Tremaine, S., 1978. *Astrophys. J.,* **222,** 850.
Goldreich, P. & Tremaine, S., 1982. *Ann. Rev. Astr. Astrophys.,* **20,** 249.
Goodman, J., Narayan, R. & Goldreich, P., 1987. *Mon. Not. R. astr. Soc.,* **225,** 695 (Paper II).
Hawley, J., 1987. *Mon. Not. R. astr. Soc.,* **225,** 677.
Hohl, F., 1971. *Astrophys. J.,* **168,** 343.
Jaroszinski, M., 1986. *Mon. Not. R. astr. Soc.,* **220,** 869.
Julian, W. H. & Toomre, A., 1966. *Astrophys. J.,* **146,** 810.
Koen, C., 1986. *Mon. Not. R. astr. Soc.,* **223,** 529.
Kojima, Y., 1986. *Progr. Theor. Phys.,* **75,** 251.
Lifshitz, E. M. & Pitaevskii, L. P., 1981. *Physical Kinetics,* p. 124, Pergamon Press, Oxford.
Lin, C. C., 1955. *The Theory of Hydrodynamic Stability,* Cambridge University Press, London.
Lin, C. C. & Shu, F., 1966. *Proc. Natl. Acad. Sci USA,* **55,** 229.
Lovelace, R. V. E., 1976. *Nature,* **262,** 649.
Lynden-Bell, D. & Kalnajs, A. J., 1972. *Mon. Not. R. astr. Soc.,* **157,** 1.
Mark, J. W. K., 1976. *Astrophys. J.,* **205,** 363.
Mouschovias, T. C., 1981. In: *Fundamental Problems in the Theory of Stellar Evolution,* p. 27, eds Sugimoto, D., Lamb, D. Q. & Schramm, D. Q., Reidel, Dordrecht, Holland.
Papaloizou, J. C. B. & Pringle, J. E., 1984. *Mon. Not. R. astr. Soc.,* **208,** 721 (PPI).

Papaloizou, J. C. B. & Pringle, J. E., 1985. *Mon. Not. R. astr. Soc.*, **213,** 799 (PPII).
Papaloizou, J. C. B. & Pringle, J. E., 1987. *Mon. Not. R. astr. Soc.*, **225,** 267.
Pierce, J. R., 1974. *Almost All About Waves,* Ch. 11, 12, MIT Press, Cambridge, Massachusetts.
Press, W. H., Flannery, B. P., Teukolsky, S. A. & Vettering, W. T., 1986. *Numerical Recipes,* p. 563, Cambridge University Press.
Shakura, N I. & Sunyaev, R. A., 1973. *Astr. Astrophys.*, **24,** 337.
Toomre, A., 1977. *Ann. Rev. astr. Astrophys.*, **15,** 437.
Toomre, A., 1981. *The Structure and Evolution of Normal Galaxies,* p. 111, eds Fall, S. M. & Lynden-Bell, D., Cambridge University Press, London.
Zurek, W. & Benz,W., 1986. *Astrophys. J.*, **308,** 123.

Appendix A: Conserved actions

A conserved action for linearized disturbances of the shearing sheet consists of a second-order density ϱ and flux $\mathbf{j}$ satisfying

$$\frac{\partial \varrho}{\partial t}+\nabla\cdot\mathbf{j}=0 \tag{A.1}$$

throughout the fluid, with

$$\mathbf{j}\cdot\hat{\mathbf{i}}=0 \tag{A.2}$$

on the boundary. The integral of ϱ over the fluid is then time-independent. The action must be expressible in terms of quadratic combinations of the first-order disturbances. Therefore, for a mode $\propto\exp(iky-i\omega t)$, equation (A.1) can be written as

$$2[\mathrm{Im}\,(\omega)]\,\varrho+\frac{\partial j}{\partial x}=0, \tag{A.3}$$

where it is understood that we use the real parts of the first-order quantities and average their second-order products over y. We write j for the x-component of $\mathbf{j}$.

One can find many conserved actions that satisfy (A.3). Ideally, we would like to find one having all of the following properties:

(1) j should vanish at the boundaries (essential if the action is conserved) for the assumed boundary condition $u=0$. In fact, we would like j to vanish even for a vanishing pressure perturbation boundary condition, which corresponds to $\Sigma'=0$ at the boundary.

(2) ϱ should change sign at corotation, and only there.

(3) ϱ should be the density of a familiar physical quantity – for example, energy or angular momentum.

(4) ϱ and j should be non-singular throughout the fluid, even for a neutral mode.

Unfortunately, we have not been able to find any single action that satisfies all four of these requirements simultaneously. In this Appendix, we shall show how Noether's theorem yields an action (equation A.16) that satisfies (1) and (3), but not (2) and (4). We shall demonstrate that this canonical action can be modified (equation A.25) so as to have property (2), but at the cost of surrendering (3). This is the action that we have found most useful in interpeting the results obtained from the Parabolic Cylinder eigenfunctions of the shearing sheet. Most of the discussion in the main text is based on this action. Finally, we shall indicate how to construct actions satisfying (1) and (4) but not (2) or (3) (equation A.27). All of these actions have the same dominant term when $\sigma\gg\Omega$ (the WKB regime), showing that they are closely related to one another.

A1 Lagrangian density

We start with the Lagrangian density

$$\mathscr{L}'=\Sigma'\left[\frac{|\,v'\,|^2}{2}+\frac{P'}{(\gamma-1)\,\Sigma'}-\Phi'+(\boldsymbol{\Omega}\times\mathbf{r}')\cdot v'\right]. \tag{A.4}$$

with $\Phi=\Omega Ax^2$. In this Appendix only, the superscript $'$ denotes that the quantity is to be evaluated in the Eulerian sense. Thus we write

$$\mathbf{r}'=\mathbf{r}+\boldsymbol{\xi}, \tag{A.5}$$

where $\mathbf{r}'$ is the Eulerian position vector, $\mathbf{r}$ is the Lagrangian position vector, i.e. the place to which a given fluid element would have been carried at a given time by the unperturbed flow, and $\boldsymbol{\xi}$ is the displacement vector of the fluid element. The velocity is

$$v'=2Ax\hat{\mathbf{j}}+\frac{d\boldsymbol{\xi}}{dt}=2Ax'\hat{\mathbf{j}}-2A\xi^x\hat{\mathbf{j}}+\frac{d\boldsymbol{\xi}}{dt}, \tag{A.6}$$

where

$$\frac{d}{dt}\equiv\frac{\partial}{\partial t}+2Ax\frac{\partial}{\partial y}. \tag{A.7}$$

The Lagrangian density $\mathscr{L}'$ must be integrated over the Eulerian area $d^2\boldsymbol{r}'$. However, the dynamical variable is $\boldsymbol{\xi}$, which it is convenient to regard as a function of $\boldsymbol{r}$ rather than $\boldsymbol{r}'$. This difficult is removed by noting that the Jacobian

$$J\equiv\left|\frac{\partial\mathbf{r}'}{\partial\mathbf{r}}\right|=\mathrm{Det}\,(\delta^i_k+\xi^i{}_{,k}) \tag{A.8}$$

relates the Eulerian and Lagrangian values of the surface density and pressure by

$$\frac{\Sigma'}{\Sigma_0}=J^{-1}, \tag{A.9}$$

and

$$\frac{P'}{P_0}=J^{-\gamma}. \tag{A.10}$$

Here Σ_0 is the mass density per Lagrangian coordinate volume, which is the same as the density in the unperturbed sheet, and P_0 is the corresponding unperturbed pressure. The Lagrangian density per unit Lagrangian volume, $\mathscr{L}$, is obtained from (A.4) by replacing Σ' with Σ_0 where it first occurs on the right-hand side, but not in the P'/Σ' term.

Expanding $\mathscr{L}$ in powers of ξ, we obtain

$$\mathscr{L}_2=\frac{\Sigma_0}{2}\left\{\left|\frac{d\boldsymbol{\xi}}{dt}\right|^2-\frac{P_0}{\Sigma_0}\left[(\gamma-1)(\xi^k{}_{,k})^2+\xi^i{}_{,j}\xi^j{}_{,i}\right]+2\varepsilon_{ijk}\Omega^j\xi^k\frac{d\xi^i}{dt}-4\Omega A(\xi^x)^2\right\}, \tag{A.11}$$

and

$$\mathscr{L}_3=\frac{\gamma P_0}{2}\xi^k{}_{,k}\left[\frac{(\gamma-2)}{3}(\xi^k{}_{,k})^2+\xi^i{}_{,j}\xi^j{}_{,i}\right]. \tag{A.12}$$

(The expression for $\mathscr{L}_3$ is valid in two dimensions only.) Commas in the subscripts of ξ represent spatial derivatives and the summation convention for repeated indices has been used.

The Euler–Lagrange equations for a mode obtained from $\mathscr{L}_2$ read:

$$(\sigma^2-4\Omega A)\,\xi^x-i2\Omega\sigma\xi^y=-c^2\xi^k{}_{,kx},$$

$$i2\Omega\sigma\xi^x+\sigma^2\xi^y=-ic^2k\xi^k{}_{,k}. \tag{A.13}$$

Here $\sigma\equiv\omega-2Akx$ and $\partial/\partial y=ik$. Note that the relations between the first-order Eulerian and Lagrangian variables for a mode are

$$u=-i\sigma\xi^x,$$

$$v=-i\sigma\xi^y-2A\xi^x,$$

$$\delta\Sigma=-\Sigma_0\xi^k{}_{,k}. \tag{A.14}$$

These follow from (A.6), (A.8), and (A.9). Using these relations we can show that equations (A.13) give back equations (2.20), (2.21), thus confirming the validity of the Lagrangian in (A.4).

A2 The canonical angular momentum

The canonical angular momentum flux, j_c, and angular momentum density, ϱ_c, are obtained by application of Noether's theorem to $\mathscr{L}_2$.

$$j_c\equiv\frac{\partial\mathscr{L}_2}{\partial(\partial\xi^k/\partial x)}\frac{\partial\xi^k}{\partial y}\rightarrow-\frac{c^2k\Sigma_0}{2}\,\mathrm{Re}\,(i\xi^k{}_{,k}\xi^{x*}), \tag{A.15}$$

and

$$\varrho_c\equiv\frac{\partial\mathscr{L}_2}{\partial(\partial\xi^k/\partial t)}\frac{\partial\xi^k}{\partial y}\rightarrow\frac{k\Sigma_0}{2}\,[\mathrm{Re}\,(\sigma)(|\xi^x|^2+|\xi^y|^2)+i\Omega(\xi^x\xi^{y*}-\xi^y\xi^{x*})], \tag{A.16}$$

where the arrows indicate evaluation for a mode, averaging over y, and an overall change of sign. Of course, ϱ_c and j_c satisfy the continuity equation (A.3), as can also be verified by application of the equations of motion (A.13). Also, j_c vanishes at the boundary, since (A.14) shows that $\xi_x=0$ when $u=0$.

The dimensions of ϱ_c are those of a momentum density, rather than an angular momentum density, because y has the dimensions of length; it is to be understood that (A.15) and (A.16) should be multiplied by the mean radius, r_0. But since r_0 is just a constant in our local approximation, we have omitted it.

We now show that the canonical angular momentum density ϱ_c is in fact identical to the true physical angular momentum density. We can identify the physical angular momentum of a particle by noting that the single particle Lagrangian,

$$L=\frac{1}{2}\left(\frac{d\mathbf{r}}{dt}\right)^2-\Phi+(\boldsymbol{\Omega}\times r)\cdot\frac{d\mathbf{r}}{dt}, \tag{A.17}$$

yields the relation

$$\frac{d}{dt}\left(\frac{dy}{dt}+2\Omega x\right)=-\frac{\partial\Phi}{\partial y}. \tag{A.18}$$

Clearly, the angular momentum per unit mass, h, is

$$h=\left(\frac{dy}{dt}+2\Omega x\right), \tag{A.19}$$

apart from the usual factor of r_0. The same result is obtained by starting with the exact expression for the angular momentum in cylindrical coordinates, transforming to a frame centred at r_0, θ_0 rotating with angular velocity $\Omega(r_0)$, making the local approximation (2.8), and taking the limit $r_0 \to \infty$. Thus the true Lagrangian angular momentum density ϱ_t can be expressed in terms of the components of the displacement vector as

$$\varrho_t = \Sigma_0 \left(\frac{d\xi^y}{dt} = 2\Omega \xi^x \right). \tag{A.20}$$

The form of ϱ_t implies that the second-order Lagrangian angular momentum density involves the second-order displacements, which we denote ξ_2^i. These are evaluated from the Euler–Lagrange equations applied to $\mathscr{L}_2 + \mathscr{L}_3$. The y equation of motion governs the evolution of the angular momentum. This equation has linear and quadratic terms in ξ. We substitute $\xi_1 + \xi_2$ for ξ, where ξ_1 satisfies equations (A.13), discard terms above the second order, and average this equation and (A.20) over y to obtain

$$2 \operatorname{Im}(\omega)\, \varrho_t = 2 \operatorname{Im}(\omega)\, \Sigma_0 [2 \operatorname{Im}(\omega)\, \xi_2^y + 2\Omega \xi_2^x] = -\frac{\partial}{\partial x} \left(\frac{\partial \mathscr{L}_3}{\partial \xi^y_{,x}} \right)$$

$$= \frac{c^2 k \Sigma_0}{2} \frac{\partial}{\partial x} \operatorname{Re}(i \xi^k_{,k} \xi^{x*}) = -\frac{\partial}{\partial x} j_c. \tag{A.21}$$

But this is exactly the equation satisfied by ϱ_c. Thus we have established that to second order, the true angular momentum ϱ_t and the canonical angular momentum ϱ_c are identical.

The quantity ϱ_c is an action that satisfies points (1) and (3) in our original list of requirements. However, unless $\Omega = 0$, there is no reason to expect that ϱ_c should change sign only at corotation. In fact, we have numerically checked that in most cases it changes sign away from corotation, often at more than one point. Another problem is that ξ_1 is generally singular at corotation (for instance, in a neutral mode a fluid element at corotation feels a constant force acting for an infinite time), so that ϱ_c and j_c are also singular there. We now try to rectify some of these difficulties.

A3 Related actions

Consider the quantity

$$j_2 = -\frac{c^2 k \Sigma_0}{2} \operatorname{Re}\left(i \frac{\sigma^*}{\sigma} \xi^k_{,k} \xi^{x*} \right). \tag{A.22}$$

Since

$$\frac{\partial (j_2 - j_c)}{\partial x} = -2 \operatorname{Im}(\omega) \frac{c^2 k \Sigma_0}{2} \operatorname{Re} \frac{\partial}{\partial x} \left(\frac{1}{\sigma} \xi^k_{,k} \xi^{x*} \right),$$

we see that j_2 is also a flux and that its associated density ϱ_2 satisfies

$$\varrho_2 = \varrho_c + \frac{c^2 k \Sigma_0}{2} \operatorname{Re} \frac{\partial}{\partial x} \left(\frac{1}{\sigma} \xi^k_{,k} \xi^{x*} \right). \tag{A.23}$$

Note that j_2 also satisfies the natural boundary conditions for the sheared sheet.

Another simple application of the equations of motion verifies that

$$\varrho_2 = \frac{k \Sigma_0}{2} \left[\frac{\operatorname{Re}(\sigma)}{|\sigma|^2} c^2 |\xi^k_{,k}|^2 - iB(\xi^x \xi^{y*} - \xi^y \xi^{x*}) \right]. \tag{A.24}$$

Thus, we can define a new conserved action density

$$\varrho_* \equiv \varrho_c + \frac{\Omega}{B}\varrho_2 = \frac{\mathrm{Re}\,(\sigma)\,k\Sigma_0}{2}\left(|\xi^x|^2+|\xi^y|^2+\frac{c^2}{|\sigma|^2}\frac{\Omega}{B}|\xi^k_{,k}|^2\right), \tag{A.25}$$

and its associated flux,

$$j_* \equiv -\frac{c^2 k\Sigma_0}{2}\,\mathrm{Re}\left[i\left(1+\frac{\Omega\sigma^*}{B\sigma}\right)\xi^k_{,k}\xi^{x*}\right]. \tag{A.26}$$

This conserved action differs from the angular momentum density by a divergence, which means we no longer satisfy point (3) of our list of requirements. But, ϱ_* changes sign only at corotation, a valuable advantage indeed, which we exploit many times in the main text to bring out the physics of the shearing sheet. Unfortunately, we do not know the physical significance, if any, of ϱ_*. It too is singular at corotation, as Fig. 8.4a and b show.

Finally, we note that if we multiply the v equation (2.26) by v^* and subtract the complex conjugate of the result, we find that

$$2\,\mathrm{Im}\,(\omega)[\mathrm{Re}\,(\sigma)|v|^2]+\frac{\partial}{\partial x}\,\mathrm{Re}\left(-iv^*\frac{dv}{dx}\right)=0. \tag{A.27}$$

This has the form of (A.3) and suggests the existence of yet another conserved action. This action density is non-singular at corotation. However, the flux in (A.27) does not vanish at the boundaries under the $u=0$ boundary condition (unless $B=0$), so this action is not conserved. (It *is* conserved if either $v=0$ or $dv/dx=0$ at the boundary, as we assumed in Section 7.2.) Appropriate terms can be added to the density and flux in (A.27) in order to make this action conserved under the $u=0$ condition, but then the density no longer changes sign at corotation.

Appendix B: Edge modes in WKB

Equation (8.2.2) shows that if $\varkappa^2>0$, there is no permitted region for modes with very small k and corotation inside the fluid, i.e. $|x_c-x_b|\leqslant 2x_b$. Nevertheless, the numerical results of Fig. 5 demonstrate that there is a neutral branch extending to $k=0$. Clearly these modes cannot be explained by equation (8.2.1). By a variation of the WKB argument, however, we can find a formula for the $k\to 0$ limit of this branch. Since k_x^2 will be negative throughout the fluid, let us define

$$\bar{k}_x \equiv +[\varkappa^2-k^2(x-x_c)^2+k^2]^{1/2}. \tag{B.1}$$

so that $\bar{k}_x^2=-k_x^2$, and seek evanescent solutions whose local decay length is $\bar{k}_x^{-1}$. A general evanescent 'WKB' solution will be of the form

$$v(x)=\Phi_-(x)\exp\left[-\int_{-x_b}^{x}\bar{k}_x(x')\,dx'\right]+\Phi_+(x)\exp\left[-\int_{x}^{x_b}\bar{k}_x(x')\,dx'\right], \tag{B.2}$$

where Φ_- and Φ_+ are slowly varying. Now in general we might expect both terms on the right-hand side of (B.2) to be present, but let us guess that the solution is purely decaying as we move away from one of the boundaries. If, for example, we choose the right-hand boundary, then $\Phi_-\equiv 0$. Then it follows directly from the boundary condition (8.4.2) that

$$x_b-x_c=\sqrt{\frac{\varkappa^2+k^2}{4B^2+k^2}}, \tag{B.3}$$

if the derivatives of Φ_+ are neglected. The nearly-vertical dotted curves in Fig. 5 were drawn using this formula.

One may ask why the above guess is justified. It follows from equations (3.9) and (2.29) that the barrier-penetration amplitude vanishes in the limit that $k \to 0$. If the distance from corotation to the left-hand wall were very large, then we would be entitled to seek a mode whose amplitude vanished far to the left. This would explain why $\Phi_- \equiv 0$. However, (8.2.1) shows that the width of the forbidden region is $\sim 2\varkappa/k$, which becomes much larger than the width of the flow for sufficiently small k, and

$$\int_{-x_b}^{x_b} \bar{k}_x(x')\,dx' \to 2\varkappa x_b, \qquad \text{as } k \to 0.$$

So it is not clear why the left-hand boundary can be neglected. Nevertheless, Fig. 5 suggests that (B.3) is exact in the limit $k \to 0$.

For $k \gg \varkappa$, the nodeless mode develops a permitted region, so we have no right to apply (B.3). In fact, it may be seen that the edge mode of Fig. 9a has a point of inflection near the right-hand wall. However, it is easily shown that (8.2.1) and (B.3) both predict that $|x_b - x_c| \to 1$ as $k \to \infty$.

The vertical notches in the neutral curves of Fig. 5 appear to trace out a curve that is consistent with these limiting behaviours, both for small and (less clearly) large k. We conclude that these notches are due to edge nodes.